

Coalescent Inference for Epidemics with Latent Periods

Isaac H. Goldstein¹, Julia Palacios¹

¹Department of Statistics, Stanford University

Abstract

Coalescent models are used to study the transmission dynamics of rapidly evolving pathogens from molecular sequence data obtained from infected individuals. However coalescent parameters, such as effective population size, offer limited interpretability for transmission dynamics. In this work, we derive a coalescent model for exposed–infected population dynamics that allows us to infer the number of infected individuals and the effective reproduction number over time from the sample genealogy. The model can be interpreted as a two-deme model in which coalescence is restricted to individuals from different demes (exposed and infected). We propose a new data-augmentation framework with Phase-type distribution for Bayesian inference of epidemiological parameters. We study the performance of our approach on simulations and apply it to re-analyze the 2014 Ebola outbreak in Liberia.

1 Introduction

It is now common practice to collect pathogen molecular sequence data obtained from infected individuals during an infectious disease outbreak or epidemic [Attwood et al., 2022, Cappello et al., 2022]. These sequences can be used to infer the shared transmission history of the pathogen among sampled individuals, represented by a genealogy, by modeling a process of mutations along the branches of the genealogy [Salemi et al., 2009, Didier and Guindon, 2024]. Typically, the genealogy is assumed to *a priori* depend on the population dynamics through two widely used classes of models: coalescent models and birth-death-sampling (BDS) models [Tavaré and Zeitouni, 2004, Stadler, 2010].

The coalescent [Kingman, 1982], initially proposed as a scaled limiting process under Wright-Fisher population dynamics, has been shown to be a good approximation to the distribution of the genealogy of a random sample of individuals under a broad class of discrete time population models [Möhle, 2000]. The coalescent model is typically parametrized in terms of the effective population size which corresponds to the population size under Wright-Fisher dynamics. However, interpretation of this parameter is more challenging under more general population dynamics. In Volz et al. [2009] and Volz [2012], the authors proposed structured coalescent models under mechanistic deterministic epidemic population dynamics, including birth-death-migration models described by ordinary differential equations (ODEs), explicitly linking the effective population size to the parameters and states of the epidemic population process. Most notably, the derivation of the coalescent model in this setting does not rely on time-scaling, limiting approximations or small sampling proportions.

The birth-death-sampling model (BDS), as in the structured coalescent, also assumes the population process is a general birth-death stochastic process. However, this approach incorporates an explicit sampling model that allows sampling in bulk with pre-specified probabilities or sampling through time according to a point process. This is one key difference with the structured coalescent that instead conditions on the number of samples at given sampling times. The BDS implementations estimate birth, death, and sampling rates, and it has been extended for multi-type processes [Kühnert et al., 2016]. In particular, the multi-type birth-death process model was recently developed to estimate epidemic population sizes in addition to population parameters [Vaughan and Stadler, 2025]. A review of some of these methods is available in Cappello et al. [2022]. Recently, King et al. [2025] proposed a framework that assumes general Markov population processes and derives a genealogical model that allows likelihood computation in a forward time fashion.

In this manuscript, we assume a birth-death-migration population process in which individuals experience a delay between being infected (exposed, E-compartment) and becoming infectious (infectious, I-compartment), a common characteristic of many real world pathogens [Xin et al., 2022, Velásquez et al., 2015]. This simplified EI population model allows us to avoid modeling the number of susceptibles. Moreover, its deterministic form governed by differential equations, has a closed form solution which is fast to compute [Goldstein et al., 2024], and that we leverage in our inferential framework. We derive the corresponding (structured) coalescent process as a thinned point process under certain assumptions. Our derivation is most similar to [Volz, 2012], however we start from stochastic population dynamics forward in time and couple it with the coalescent backwards in time conditioned on observed samples at given sampling times. As in Volz [2012], our derivation does not rely on scaling, limiting approximations or small sampling proportions.

Multiple approaches for Bayesian inference of population parameters under the aforementioned models have been proposed in recent years, including Markov chain Monte Carlo (MCMC), and sequential Monte Carlo approaches. The methods developed in Volz [2012], Müller et al. [2017], Volz and Siveroni [2018], infer population parameters under a wide range of deterministic structured population processes by integrating over the states of sampled lineages. This is made tractable by approximating the likelihood assuming lineage states are independent [Müller et al., 2017, Volz and Siveroni, 2018]. For the simplest epidemic process, the SIR stochastic model, which assumes a single class of infectious individuals with no latent period, Rasmussen et al. [2011] used particle MCMC to infer the latent number of infectious individuals. More recently, Tang et al. [2023] used a linear noise approximation, an approximate continuous stochastic process, to model the latent number of infectious individuals in a more computationally efficient manner.

In this manuscript, we develop a Bayesian data augmentation method to estimate model parameters and population size trajectories from a genealogy. We target the posterior distribution of model parameters, population size trajectories, and compartment states of sampled lineages at observed times (coalescent and sampling times). For the augmented likelihood we recast the coalescent density as phase type distributions [Zeng et al., 2021, Hobolth et al., 2024]. Compartment states of sampled lineages at observed times are sampled exactly, while population parameters and population size trajectories are sampled using MCMC. In our implementation, we assume the reproduction number is a piece-wise constant trajectory modeled with a Gaussian Markov random field prior. We test our new method on simulated epidemics and apply our model to the 2014 Ebola outbreak in Liberia.

2 Methods

2.1 Phylogeny as Data

Throughout this paper, we will assume a fixed genealogy as the “observed data”. This genealogy is normally estimated from molecular sequences, or from previous studies. The relevant characteristics of the genealogy for our model are the times of coalescence and the times when lineages are sampled, as well as the specific type of event at those times. We represent the times of events with the vector $\mathbf{t} = \{t_0, \dots, t_n\}$, where n is the total number of coalescent and sampling times, and $t_0 < \dots < t_n$. Further, these times are measured in units backwards in time, so that $t_0 = 0$ is the present time, and t_N is the time of the most recent common ancestor of the sampled lineages (Figure 1(C)). Let the vector $\mathbf{x} = \{x_0, \dots, x_n\}$ be the types of these events, where if $x_i = 1$, the event at time t_i is a coalescent event and if $x_i = 0$ the event at time t_i is a sampling event.

2.2 The EI Population Model

The EI population model assumes an epidemic evolving in forward time, with the population split into two compartments, individuals who are infected but not infectious (E), and individuals who are infectious (I). To avoid confusion, we will use the letter u to represent forward time, and the letter t for backwards time. The EI model is a bivariate continuous time Markov jump process $\mathbf{H}(u) = (E(u), I(u))$, that satisfies:

$$\begin{aligned} P(\mathbf{H}(u + du) = (e + 1, i) \mid \mathbf{H}(u) = (e, i)) &= \alpha(u)idu + o(du), \\ P(\mathbf{H}(u + du) = (e - 1, i + 1) \mid \mathbf{H}(u) = (e, i)) &= \gamma edu + o(du), \\ P(\mathbf{H}(u + du) = (e, i - 1) \mid \mathbf{H}(u) = (e, i)) &= \nu idu + o(du) \\ P(\mathbf{H}(u + du) = (e, i) \mid \mathbf{H}(u) = (e, i)) &= 1 - (\alpha(u)i + \gamma e + \nu i)du + o(du). \end{aligned}$$

Here γ is interpreted as the inverse of the mean latent period, ν is the inverse of the mean infectious period, and $\alpha(u)$ is the time-varying per-capita number of new infections per unit time. Throughout we will assume $\alpha(u)$ is a continuous function. In keeping with terminology from prior phylogenetics literature, we will refer to the event when $\mathbf{H}(u + du) = (e + 1, i)$ as a birth, and the event when $\mathbf{H}(u + du) = (e - 1, i + 1)$ as a migration. The effective reproduction number (which is often denoted R_t , but for consistency we will use R_u), is then defined as $R_u = \alpha(u)/\nu$. Appendix Section A.1 describes in more detail the differences between the EI population model and the more traditional SEIR population model.

Although the $\mathbf{H}(u)$ process only keeps track of the number of individuals in each compartment, we can represent the population history by an EI population genealogy in which the event $\mathbf{H}(u + du) = (e + 1, i)$

corresponds to a birth when a uniformly sampled I lineage (red) splits into two lineages: one E (blue) lineage and one I (red) lineage in the population genealogy; and the event $\mathbf{H}(u + du) = (e - 1, i + 1)$ corresponds to a migration when a uniformly sampled E (blue) lineage becomes an I (red) lineage; and the event $\mathbf{H}(u + du) = (e, i - 1)$ corresponds to a death when a uniformly sampled I lineage is pruned in the population genealogy. Figure 1(A) shows a realization of the process from state $\mathbf{H}(0) = (0, 1)$ to $\mathbf{H}(T) = (2, 2)$, and a corresponding population genealogy with lineages colored according to their state (exposed or infectious). For illustration purposes only, tree tips are labeled. We note that even when tips are not labeled in the population genealogy, many tree shapes correspond to the same $\mathbf{H}(u)$ trajectory (for example lineage 4 could have been chosen to split at time u_4 giving rise to a different tree shape). For our likelihood expressions we focus on $\mathbf{H}(u)$ realizations. The corresponding population genealogy likelihood would include a combinatorial factor that accounts for the number of different tree shapes. Similarly, the corresponding population labeled genealogy likelihood would include a combinatorial factor that accounts for the number of different labeled tree topologies.

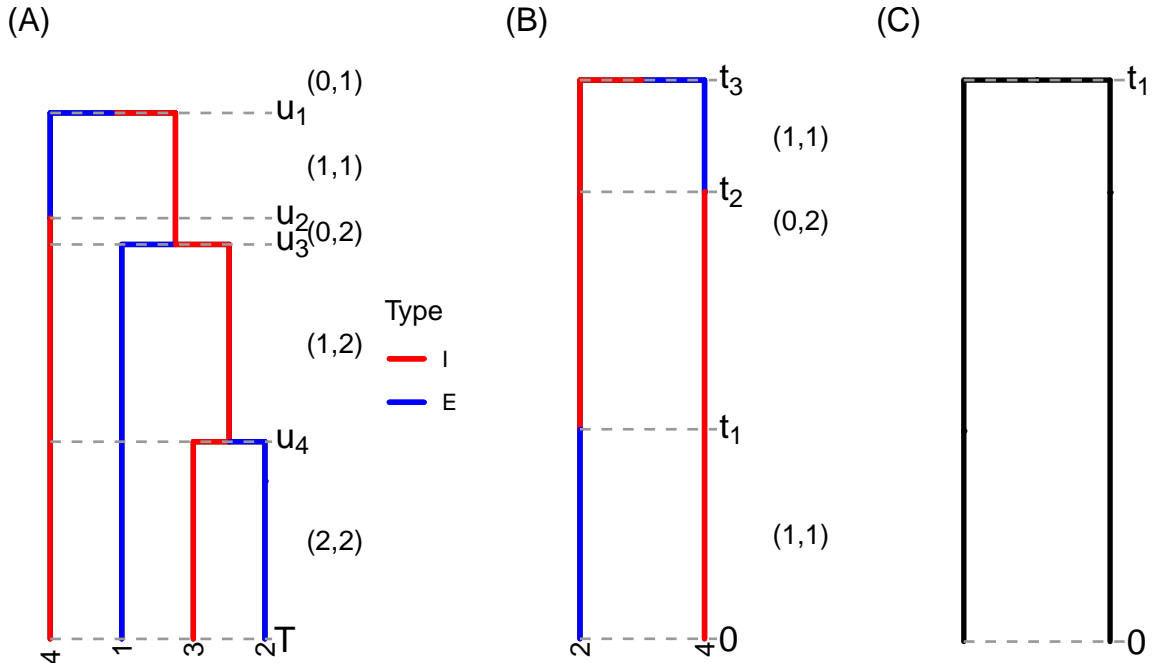


Figure 1: (A) A realization of the EI population process with initial state $\mathbf{H}(0) = (0, 1)$ and end state $\mathbf{H}(T) = (2, 2)$, together with one corresponding population genealogy. Given $C(T) = (n_E(T), n_I(T)) = (1, 1)$, one E lineage (blue) and one I lineage (red) are sampled at time T . Figure (B) shows the corresponding EI sampled process (and sample genealogy) when tips 4 and 2 are chosen. Here time increases from tips to root, with $t_3 = T$. In (C), only coalescent events (births) of sampled lineages are observed.

2.3 The EI sampled genealogy

Assume a population that evolves (forward in time) according to the EI population model started at $\mathbf{H}(0) = (0, 1)$. Given the full realization $(\mathbf{H}(u))_{u \in [0, T]}$ until present day at time T , we sample uniformly at random n_E from the total $E(T)$ of exposed individuals at time T , and n_I from the total $I(T)$ of infected individuals. We then trace back the number of sampled individuals in each compartment over time to obtain the sample EI continuous time process $\mathbf{C}(u) = (n_E(u), n_I(u))$. Figure 1(B) shows the genealogy of samples 2 and 4 obtained by sampling $n_E = 1$ and $n_I = 1$ exposed and infected lineages at time T from the realization of Figure 1(A). For illustration purposes in Figure 1, we have labeled tips 1 to 4 and fixed a particular tree shape, however we note that our $\mathbf{H}(u)$ process only counts the number of E and I individuals over time.

In this section we first derive the exact likelihood of the joint process of $\mathbf{H}(u)$, $\mathbf{C}(u)$, then an approximate likelihood of $\mathbf{H}(u)$, $\mathbf{C}(u)$ when the population counts are approximated by a piecewise constant function, and

finally we propose a backwards time process $\tilde{\mathbf{C}}(t)$, whose likelihood is the thinned likelihood of the joint approximated process. The likelihood of the backwards time process is what we will use for inference.

The sample's transition history $(\mathbf{C}(u))_{u \in [0, T]}$ is referred to as the fully observed EI coalescent trajectory. $(\mathbf{C}(u))_{u \in [0, T]}$ can also be constructed sequentially by first generating $(\mathbf{H}(u))_{u \in [0, T]}$ and then sampling the discrete (lazy) jump chain $\{\mathbf{C}(u_i)\}_{i=k}^1$ from tips to root, assuming an initial state $\mathbf{C}(T) = (n_E(T), n_I(T))$. We will show how to do this through the following examples.

Example 1a. Assume we are given the EI realization shown in Figure 1(A) and that $n_E(T) = 1$ and $n_I(T) = 1$, that is $\mathbf{C}(T) = (1, 1)$. Then, given that a birth occurs at u_4 , this event is observed in the sample as a coalescent event with probability $P(\mathbf{C}(u_4) = (0, 1) \mid \mathbf{C}(T) = (1, 1), (\mathbf{H}(u))_{u \in [0, T]}) = 1/4$, since we can pick the E to be in the sample out of the two (w.p. 1/2) and similarly for I. Alternatively, u_4 could be observed in the sample as a migration event if only the E lineage involved in u_4 is in the sample (lineage 2 in Figure 1(A)). This event also has probability $P(\mathbf{C}(u_4) = (0, 2) \mid \mathbf{C}(T) = (1, 1), (\mathbf{H}(u))_{u \in [0, T]}) = 1/4$. This possibility is shown in Figure 1(B), where lineage 2 changes from blue to red at time t_1 in backwards time which is equal to time u_4 in forwards time.

The probability that u_3 is in the sample as a coalescent event is the probability that the E lineage involved is in the sample (w.p. 1/2) and the I lineage involved in u_4 is in the sample (w.p 1/2), therefore u_3 is in the sample with probability $P(\mathbf{C}(u_3) = (0, 1) \mid \mathbf{C}(T) = (1, 1), (\mathbf{H}(u))_{u \in [0, T]}) = 1/4$. Similarly u_2 is in the sample (as migration) with probability $P(\mathbf{C}(u_2) = (1, 1) \mid \mathbf{C}(T) = (1, 1), (\mathbf{H}(u))_{u \in [0, T]}) = 1/2$, and finally, u_1 is in the sample (as coalescent) with probability $P(\mathbf{C}(u_1) = (0, 1) \mid \mathbf{C}(T) = (1, 1), (\mathbf{H}(u))_{u \in [0, T]}) = 1/2$.

Example 1b. We will now compute the same probability for u_3 in a coalescent manner (sequentially from tips to root). Conditioned on $\mathbf{C}(T) = (1, 1)$, $\mathbf{C}(u_4)$ can take the values $(1, 1)$, $(0, 2)$, and $(0, 1)$ with probabilities 1/2, 1/4 and 1/4 respectively. However u_3 cannot be a coalescent in the sample if $\mathbf{C}(u_4)$ takes the values $(0, 2)$, $(0, 1)$. Therefore, conditioned on $\mathbf{C}(u_4) = (1, 1)$, u_3 is a coalescent in the sample with probability 1/2, and $P(\mathbf{C}(u_3) = (0, 1) \mid \mathbf{C}(T) = (1, 1), \mathbf{H}(u)) = P(\mathbf{C}(u_3) = (0, 1) \mid \mathbf{C}(u_4) = (1, 1), \mathbf{H}(u)) \times P(\mathbf{C}(u_4) = (1, 1) \mid \mathbf{C}(T) = (1, 1), \mathbf{H}(u)) = 1/4$.

In practice, we assume that we only sample infectious individuals and so $\mathbf{C}(T) = (0, n_I(T))$. Modeling $\mathbf{H}(u)$ as a Marked point process, let $m(u) \in \{1, 2, 3\}$ mark whether the transition type at time u is a birth, migration, or death. Then, the $\{\mathbf{C}(u_i)\}$ jump chain is governed by the following transition probabilities.

Coalescence of sampled E and I lineages:

$$P(\mathbf{C}(u_i) = \mathbf{C}(u_{i+1}) + (-1, 0) \mid \mathbf{C}(u_{i+1}), m(u_i) = 1, (\mathbf{H}(t))_{t \in [0, T]}) = \frac{n_E(u_{i+1})}{E(u_i)} \frac{n_I(u_{i+1})}{I(u_i)} \quad (1)$$

Given $(\mathbf{H}(u))_{u \in [0, T]}$ and a birth transition at time u_i ($m(u_i) = 1$), we proceed backwards in time choosing two lineages uniformly at random to coalesce. Given there are $n_E(u_{i+1})$ sampled E lineages out of the total of $E(u_{i+1}) = E(u_i)$, and $n_I(u_{i+1})$ I sampled lineages out of the total of $I(u_{i+1}) = I(u_i)$, this coalescence will involve two lineages in the sample with probability given in Eq. 1. Recall that according to section 2.2, $I(t)$ and $E(t)$ are both right continuous functions.

In this case, the new state in the $\mathbf{C}(u)$ chain becomes $\mathbf{C}(u_i) = (n_E(u_{i+1}) - 1, n_I(u_{i+1}))$. One E and one I lineage merge to become one I lineage and so the number of I lineages in the sample does not change.

Coalescence of sampled E and non-sampled I lineages:

$$P(\mathbf{C}(u_i) = \mathbf{C}(u_{i+1}) + (-1, 1) \mid \mathbf{C}(u_{i+1}), m(u_i) = 1, (\mathbf{H}(t))_{t \in [0, T]}) = \frac{n_E(u_{i+1})}{E(u_i)} \frac{I(u_i) - n_I(u_{i+1})}{I(u_i)}. \quad (2)$$

Same conditioning as before, but coalescence occurs between an E lineage in the sample and an I lineage not in the sample. In this case, the E lineage in the sample becomes an I lineage after merging with I, and so $\mathbf{C}(u_i) = (n_E(u_{i+1}) - 1, n_I(u_{i+1}) + 1)$. We refer to this event as coalescent migration.

Coalescence of non-sampled E and non-sampled I lineages or coalescence of non-sampled E and sampled I:

$$P(\mathbf{C}(u_i) = \mathbf{C}(u_{i+1}) \mid \mathbf{C}(u_{i+1}), m(u_i) = 1, (\mathbf{H}(t))_{t \in [0, T]}) = 1 - \frac{n_E(u_{i+1})}{E(u_i)}. \quad (3)$$

Same conditioning as before, but coalescence occurs between two lineages that are not in the sample or between an I lineage in the sample and an E lineage not in the sample. In both cases, the state of $\mathbf{C}(u_i)$ does not change.

Migration in the sample:

$$P(\mathbf{C}(u_i) = \mathbf{C}(u_{i+1}) + (1, -1) \mid \mathbf{C}(u_{i+1}), m(u_i) = 2, (\mathbf{H}(t))_{t \in [0, T]}) = \frac{n_I(u_{i+1})}{I(u_i)}. \quad (4)$$

Given $(\mathbf{H}(u))_{u \in [0, T]}$, $\mathbf{C}(u_{i+1})$, and a migration transition at time u_i ($m(u_i) = 2$), one I lineage in the sample is selected out of all $I(u_{i+1})$ to become an E lineage (in the sample). In this case, the state becomes $\mathbf{C}(u_i) = (n_E(u_{i+1}) + 1, n_I(u_{i+1}) - 1)$.

Migration not in the sample:

$$P(\mathbf{C}(u_i) = \mathbf{C}(u_{i+1}) \mid \mathbf{C}(u_{i+1}), m(u_i) = 2, (\mathbf{H}(t))_{t \in [0, T]}) = 1 - \frac{n_I(u_{i+1})}{I(u_i)}. \quad (5)$$

Same conditioning as before, but migration occurs in a lineage not in the sample.

We can now derive the likelihood of the joint process: the EI population process $\mathbf{H}(u)$ (forward in time), and the fully observed EI coalescent jump process $\{\mathbf{C}(u_i)\}$ (proceeding backwards from time T to 0), conditioned on $\mathbf{H}(0) = (0, 1)$ and $\mathbf{C}(T) = (0, n_I(T))$. We note that $\mathbf{C}(T)$ imposes constraints in the EI population process as this implies $I(T) \geq n_I(T)$. In particular, having $n_I(T) > 0$ samples implies that the EI population process did not go extinct in $[0, T]$. Thus, the likelihood of the EI population process $(\mathbf{H}(u))_{u \in [0, T]}$ conditioned on $\mathbf{H}(0) = (0, 1)$ and $I(T) \geq n_I(T)$ is:

$$\mathcal{L}^*(\lambda, \nu, \alpha; \mathbf{H}(u)) = e^{-\int_{u_k}^T \lambda(u) du} \prod_{i=1}^k f(u_i \mid u_{i-1}) \frac{\lambda(m, u_i)}{\lambda(u_i)} \frac{\mathbb{1}(I(T) \geq n_I(T))}{P(I(T) \geq n_I(T) \mid \mathbf{H}(0))}, \quad (6)$$

where $u_0 = 0$, $\lambda(u_i) = (\alpha(u_i) + \nu)I(u_{i-1}) + \gamma E(u_{i-1})$ and $f(u_i \mid u_{i-1}) = \lambda(u_i) e^{-\int_{u_{i-1}}^{u_i} \lambda(u) du}$ is the conditional density evaluated at u_i . Assuming $\alpha(u)$ is a continuous function, and $I(u), E(u)$ are right continuous, then according to Section 2.2, the jump (or mark) probabilities are:

$$\frac{\lambda(m, u_i)}{\lambda(u_i)} = P(\mathbf{H}(u_i) \mid \mathbf{H}(u_{i-1})) = \begin{cases} \frac{\alpha(u_i)I(u_{i-1})}{(\alpha(u_i) + \nu)I(u_{i-1}) + \gamma E(u_{i-1})} & \text{if } m = 1 \text{ (birth)} \\ \frac{\gamma E(u_{i-1})}{(\alpha(u_i) + \nu)I(u_{i-1}) + \gamma E(u_{i-1})} & \text{if } m = 2 \text{ (migration)} \\ \frac{\nu I(u_{i-1})}{(\alpha(u_i) + \nu)I(u_{i-1}) + \gamma E(u_{i-1})} & \text{if } m = 3 \text{ (death).} \end{cases}$$

The likelihood of the joint process is then:

$$\begin{aligned} \mathcal{L}^*(\lambda, \nu, \alpha; \mathbf{H}(u), \mathbf{C}(u)) &= e^{-\int_{u_k}^T \lambda(u) du} \prod_{i=1}^k f(u_i \mid u_{i-1}) \frac{\lambda(m, u_i)}{\lambda(u_i)} P(\mathbf{C}(u_1), \dots, \mathbf{C}(u_k) \mid \{\mathbf{H}(u_i)\}_{i=1}^k, \mathbf{C}(T)) \times \\ &\quad \frac{\mathbb{1}(I(T) \geq n_I(T))}{P(I(T) \geq n_I(T) \mid \mathbf{H}(0))}, \end{aligned} \quad (7)$$

Re-arranging terms in Eq. 7, simplifying, and expressing the conditional joint distribution of $\{\mathbf{C}(u_i)\}_{i=1}^k$ as a product of conditional probabilities, we get:

$$\begin{aligned} \mathcal{L}^*(\lambda, \nu, \alpha; \mathbf{H}(u), \mathbf{C}(u)) &= e^{-\int_0^{u_1} \lambda(u) du} \prod_{i=k}^1 P(\mathbf{C}(u_i) \mid \mathbf{C}(u_{i+1})) \lambda(m, u_i) e^{-\int_{u_i}^{u_{i+1}} \lambda(u) du} \frac{\mathbb{1}(I(T) \geq n_I(T))}{P(I(T) \geq n_I(T) \mid \mathbf{H}(0))} \\ &= e^{-\int_0^{u_1} \lambda(u) du} \prod_{i=k}^1 \mu(M, u_i) e^{-\int_{u_i}^{u_{i+1}} \lambda(u) du} \frac{\mathbb{1}(I(T) \geq n_I(T))}{P(I(T) \geq n_I(T) \mid \mathbf{H}(0))}, \end{aligned} \quad (9)$$

where $u_{k+1} = T$, and $\mu(M, u_i) = P(\mathbf{C}(u_i) \mid \mathbf{C}(u_{i+1}))\lambda(m, u_i)$ with M denoting a new mark that considers both the m mark of the population EI process and the mark of the coalescent jump process (corresponding to transition probabilities of Eqs. 1-5). In particular, $M \in \{1, \dots, 6\}$ corresponds to 1: population birth and sample coalescent, 2: population birth and sample migration (E to I backwards transition), 3: birth that does not change coalescence state, 4: Migration in the population (E to I forwards) and in the sample (I to E backwards), 5: Migration in the population but not in the sample, and 6: population death. To be more precise, these marked rates are:

$$\mu(M, u_i) = \begin{cases} \alpha(u_i)I(u_{i-1}) \frac{n_E(u_{i+1})}{E(u_i)} \frac{n_I(u_{i+1})}{I(u_i)} & \text{if } M(u_i) = 1 \text{ (birth and coalescent)} \\ \alpha(u_i)I(u_{i-1}) \frac{n_E(u_{i+1})}{E(u_i)} \frac{I(u_i) - n_I(u_{i+1})}{I(u_i)} & \text{if } M(u_i) = 2 \text{ (birth and coalescent migration)} \\ \alpha(u_i)I(u_{i-1}) \left(1 - \frac{n_E(u_{i+1})}{E(u_i)}\right) & \text{if } M(u_i) = 3 \text{ (birth and off-sample event)} \\ \gamma E(u_{i-1}) \frac{n_I(u_{i+1})}{I(u_i)} & \text{if } M(u_i) = 4 \text{ (migration in the sample)} \\ \gamma E(u_{i-1}) \left(1 - \frac{n_I(u_{i+1})}{I(u_i)}\right) & \text{if } M(u_i) = 5 \text{ (migration not in the sample)} \\ \nu I(u_{i-1}) & \text{if } M(u_i) = 6 \text{ (death).} \end{cases}$$

As we will show in the proof of Theorem 2.1 below, it is convenient to re-express $\mu(M, u_i)$ in terms of the population sizes $I(u_i)$ and $E(u_i)$. Since knowing the type of the transition allows us to go from $I(u_{i-1})$ to $I(u_i)$ (and similarly for $E(u_{i-1})$), we get:

$$\mu(M, u_i) = \begin{cases} \alpha(u_i)I(u_i) \frac{n_E(u_{i+1})}{E(u_i)} \frac{n_I(u_{i+1})}{I(u_i)} & \text{if } M(u_i) = 1 \text{ (birth and coalescent)} \\ \alpha(u_i)I(u_i) \frac{n_E(u_{i+1})}{E(u_i)} \frac{I(u_i) - n_I(u_{i+1})}{I(u_i)} & \text{if } M(u_i) = 2 \text{ (birth and coalescent migration)} \\ \alpha(u_i)I(u_i) \left(1 - \frac{n_E(u_{i+1})}{E(u_i)}\right) & \text{if } M(u_i) = 3 \text{ (birth and off-sample event)} \\ \gamma(E(u_i) + 1) \frac{n_I(u_{i+1})}{I(u_i)} & \text{if } M(u_i) = 4 \text{ (migration in the sample)} \\ \gamma(E(u_i) + 1) \left(1 - \frac{n_I(u_{i+1})}{I(u_i)}\right) & \text{if } M(u_i) = 5 \text{ (migration not in the sample)} \\ \nu(I(u_i) + 1) & \text{if } M(u_i) = 6 \text{ (death).} \end{cases}$$

When there is a birth in the (forward) population process at time u_i , the corresponding rate is $\alpha(u_i)I(u_i^-) = \alpha(u_i)I(u_{i-1})$ and the number of I lineages does not change at u_i , i.e. $I(u_i) = I(u_i^-)$ as only one E lineage is created. Similarly, when there is a migration E to I, the number of E lineages decreases by 1 and so $E(u_i^-) = E(u_i) + 1$.

Although the likelihood of Eq. 9 has the same factorization of a time-reversal Markov process, this does not correspond to the time-reversal of the original EI population process with coalescent markings. A time-reversal expression would require calculation of the marginal of the population EI process at present time T and of transition probabilities as functions of multiple marginals. We will now consider the scenario where the EI population sizes can be approximated by the corresponding deterministic model governed by ordinary differential equations. Then, assuming we are given $\tilde{I}(u)$ and $\tilde{E}(u)$ (approximated at a pre-specified grid points in $[0, T]$), the likelihood corresponds to the likelihood of an Inhomogeneous Marked Poisson Process, that is:

$$\tilde{\mathcal{L}}(\lambda, \nu, \alpha; k, \{u_i, M(u_i)\}_{i=1}^k) = e^{-\int_0^{u_1} \tilde{\lambda}(u) du} \prod_{i=k}^1 \tilde{\mu}(M, u_i) e^{-\int_{u_i}^{u_{i+1}} \tilde{\lambda}(u) du} \mathbb{1}(\tilde{I}(T) \geq n_I(T)), \quad (10)$$

where $\tilde{\lambda}(u)$ and $\tilde{\mu}(M, u)$ are based on $\tilde{I}(u)$ and $\tilde{E}(u)$. We decouple the values of $I(u)$ and $E(u)$ from the jumps of the point process in order to propose an approximate backwards time point process. Without this assumption, the backwards time process is a lazy discrete process (Eqs. 1-5), a jump chain with possible jumps at times where $E(u)$ and $I(u)$ changed. Instead, we propose an approximate backwards time point process $\tilde{\mathbf{C}}(t)$, whose likelihood is derived from Equation 10.

Theorem 2.1. *Let $\tilde{I}(t)$ and $\tilde{E}(t)$ approximate the EI population trajectories $I(t)$ and $E(t)$ on $[0, T]$, then conditioned on $\tilde{I}(t)$ and $\tilde{E}(t)$, the continuous time processes $\tilde{\mathbf{C}}(t)$ is described by the following infinitesimal*

transition probabilities:

$$\begin{aligned}
P(\tilde{\mathbf{C}}(t+dt) = (n_E - 1, n_I) | \tilde{\mathbf{C}}(t) = (n_E, n_I)) &= n_E \times n_I \times \frac{\alpha(t)}{\tilde{E}(t)} dt + o(dt). \\
P(\tilde{\mathbf{C}}(t+dt) = (n_E + 1, n_I - 1) | \tilde{\mathbf{C}}(t) = (n_E, n_I)) &= n_I \times \frac{\gamma(\tilde{E}(t) + 1)}{\tilde{I}(t)} dt + o(dt) \\
P(\tilde{\mathbf{C}}(t+dt) = (n_E - 1, n_I + 1) | \tilde{\mathbf{C}}(t) = (n_E, n_I)) &= \mathbb{1}(\tilde{I}(t) > n_I(t)) \times n_E \times (\tilde{I}(t) - n_I) \times \frac{\alpha(t)}{\tilde{E}(t)} dt + o(dt).
\end{aligned}$$

Here $\mathbb{1}(\tilde{I}(t) > n_I(t))$ is the indicator function which is 1 when $\tilde{I}(t) > n_I(t)$ and 0 otherwise.

Proof. We first change the direction of time (from present time 0 at the tips to the root) and express the likelihood of Eq. 10 in terms of $t_i = T - u_{k-i+1}$ for all $i = 0, \dots, k+1$

$$\mathcal{L}(\tilde{I}, \tilde{E}, \nu, \alpha; k, \{t_i, M(t_i)\}_{i=1}^k) = e^{-\int_{t_k}^T \tilde{\lambda}(t) dt} \prod_{i=1}^k \tilde{\mu}_-(M, t_i) e^{-\int_{t_{i-1}}^{t_i} \tilde{\lambda}(t) dt} \mathbb{1}(\tilde{I}(0) \geq n_I(0)), \quad (11)$$

where $\tilde{\mu}_-(M, t_i)$ (and hence $\tilde{\lambda}(u)$) is expressed in terms of approximated population trajectories $\tilde{I}(t_i)$, $\tilde{E}(t_i)$, which are left continuous in reverse time (from present time 0 to the past T), and $\alpha(t_i)$ evaluated at t_i , and coalescent lineage counts $n_E(t_{i-1})$, $n_I(t_{i-1})$. In particular, the background intensity function

$$\tilde{\lambda}(t) = (\alpha(t) + \nu)\tilde{I}(t) + \gamma\tilde{E}(t) + \gamma + \nu$$

is predictable [Daley and Vere-Jones, 2003]. Let $O = \{t_1^*, t_2^*, \dots, t_N^*\} \subset \{t_1, \dots, t_k\}$ denote the ordered subset of event times with marks 1, 2, and 4. Then the restricted point process to O is the EI sample continuous-time coalescent process corresponding to the thinned Poisson process [Kingman, 1992] with total rate

$$\lambda_c(t) = \frac{\alpha(t)\tilde{I}(t)}{\tilde{E}(t)} n_E(t^-) + \frac{\gamma(\tilde{E}(t) + 1)}{\tilde{I}(t)} n_I(t^-),$$

and the corresponding marks have transition rates that correspond to the desired result. \square

The likelihood of the $\tilde{\mathbf{C}}(t)$ process is then the corresponding likelihood of a continuous-time Markov chain with rates described in Theorem 2.1. In our implementation, we allow tips to have different sampling times (heterochronous sampling). Accommodating for heterochronous sampling is equivalent to allowing the $\mathbf{C}(t)$ chain to have deterministic jumps at sampling times. Finally, the corresponding likelihood for the EI sample genealogy is the $\tilde{\mathbf{C}}(t)$ likelihood divided by a combinatorial factor that counts the number of labeled (and colored) tree topologies. In the next sections, we only consider the likelihood of $\tilde{\mathbf{C}}(t)$.

2.4 Augmented Likelihood

Although our data is an unmarked genealogy where we only observe coalescent times (times of type 1 events) such as in Figure 1(C), our data-augmentation scheme allows us to sample the states $\tilde{\mathbf{C}}(t_i)$ at a discrete grid of N times. We note that we do not augment the full realization of the $\tilde{\mathbf{C}}(t)$ process, instead we only sample the states at the grid times.

For a partially observed $\tilde{\mathbf{C}}(t)$, the likelihood contribution of a coalescent interval can be written as a multiple risk phase type density (see Hobolth et al. [2024] for an overview of phase type distributions for coalescent models, and Lindqvist [2023] for a general review of competing risk phase-type distributions). Under this framework, starting with k lineages, the next coalescence is the first time the process reaches a state with only $k-1$ lineages, where each of the states with $k-1$ lineages are considered absorbing states.

Define matrix A_k , a $k+1 \times k+1$ matrix which contains the rates of transitioning between states with k lineages ordered so that the first row and column correspond to having k lineages in state I, decreasing by 1 from left to right and top to bottom. In this case, there are $k+1$ total states, as there can be between 0 and k lineages in state I (vice versa state E). Let matrix L_k be a $k+1 \times k-1$ matrix which contains the rates

of transition to any of the $k - 1$ possible coalescent states (any state with at least one lineage in each state can transition to coalescence, there are $k - 1$ such states). Then the full intensity matrix \mathbf{Q}_k describing the coalescent process from k lineages to $k - 1$ lineages is

$$\mathbf{Q}_k = \begin{bmatrix} \mathbf{A}_k & \mathbf{L}_k \\ \mathbf{0} & \mathbf{0} \end{bmatrix}. \quad (12)$$

In the case when the rates of \mathbf{Q}_k are constant, the transition matrix is simply $\exp \mathbf{Q}_k t$, which by properties of block matrices, is

$$\exp \mathbf{Q}_k t = \begin{bmatrix} \exp \mathbf{A}_k t & \mathbf{A}^{-1} k (\exp \mathbf{A}_k t - \mathbf{I}) \mathbf{L}_k \\ \mathbf{0} & \mathbf{1} \end{bmatrix}. \quad (13)$$

In pursuit of model simplicity, we will assume the rates are indeed constant between coalescent events. Let s_i index the $k + 1$ possible states of $\tilde{\mathbf{C}}(t_i)$ with k lineages. In particular, we define s_i so that $s_i - 1$ is the number of lineages in state E (alternatively $k - s_i + 1$ is the number of lineages in state I). Then the augmented likelihood contribution starting from time t_{i-1} in state s_{i-1} ending in coalescence at time t_i and state s_i is

$$f_{s_{i-1}s_i}(t_i - t_{i-1}, x_i = 1) = \mathbf{e}_{s_{i-1}}^T \exp\{\mathbf{A}(t_i - t_{i-1})\} \mathbf{l}_{s_i} \quad (14)$$

where \mathbf{l}_{s_i} is the s_i th column of \mathbf{L} . In the case of heterochororous sampling we also require augmented likelihood contributions for sampling events. These contributions are calculated using the entries of $\exp \mathbf{A}(t_i - t_{i-1})$. Suppose at time t_{i-1} the process is in state s_{i-1} and the next time t_i is a sampling event, then the process is in one of the $k + 1$ transient states just before sampling, and after sampling the total number of lineages is increased deterministically by the number of samples collected at t_i . The likelihood contribution of such an event is $\exp \mathbf{Q}(t_i - t_{i-1})$ corresponding to the transition from s_{i-1} to a transient state s_i in the time $t_i - t_{i-1}$. We can write this contribution explicitly as

$$f_{s_{i-1}s_i}(t_i - t_{i-1}, x_i = 0) = \exp \mathbf{A}(t_i - t_{i-1})_{s_{i-1}, s_i}.$$

Let the states of the grid points be $\mathbf{s} = \{s_0, \dots, s_N\}$, then the augmented likelihood can be written as

$$P(\mathbf{t}, \mathbf{x}, \mathbf{s} | \alpha, \gamma, \tilde{\mathbf{E}}, \tilde{\mathbf{I}}) = \prod_{i=1}^N f_{s_{i-1}s_i}(t_i - t_{i-1}, x_i).$$

The matrix exponential of \mathbf{A}_k is not available in closed form. For full matrix exponentials, we use the scaling and squaring method of Higham [2005] to numerically calculate the desired matrix. When only the action of the matrix exponential is needed for large matrices and small time steps, we use a Krylov subspace method [Niesen and Wright, 2009]. We use the methods as implemented in the `julia` package `ExponentialUtilities.jl` [Rackauckas and Nie, 2017].

2.5 Posterior Inference

2.5.1 Coalescent EI Model Structure

We place a random walk prior on the grid of time-varying effective reproduction numbers R_u :

$$\begin{aligned} R_0 &\sim \text{Log-Normal}(\mu_0, \sigma_0), \\ \sigma &\sim \text{Log-Normal}(\mu_{rw}, \sigma_{rw}), \\ \log(R_{k_i}) | R_{k_{i-1}}, \sigma &\sim \text{Normal}(\log(R_{k_{i-1}}), \sigma). \end{aligned}$$

Let $\Theta = (\gamma, \nu, I(0), E(0))$, $\mathbf{R} = (R_0, \dots, R_{k_M})$ be the vector of effective reproduction number values, $\tilde{\mathbf{E}}$ and $\tilde{\mathbf{I}}$ are the vectors of population counts. We augment the observed times \mathbf{t} with additional pre-specified times which are the times at which the effective reproduction number is chosen to change. For this paper, we allow R_u to change every seven days. In terms of the augmented likelihood, these additional grid times are treated as sampling events where the number of sampled lineages is 0. In the Appendix, we describe an alternative formulation of the model which augments the states only at the times of sampling and coalescence. Let

$\mathbf{s}^* = (s_0, \dots, s_N)$ be the states of $\tilde{\mathbf{C}}(t)$ at the pre-specified grid times $t^* = (t_0, \dots, t_N)$ which includes \mathbf{t} . Let \mathbf{x}^* be the corresponding vector of event types. The target posterior distribution is

$$P(\mathbf{R}, \mathbf{s}^*, \boldsymbol{\Theta}, \tilde{\mathbf{E}}, \tilde{\mathbf{I}}, \sigma \mid \mathbf{x}^*, \mathbf{t}^*).$$

We estimate the target posterior via Metropolis within Gibbs sampling, by first sampling from

$$P(\mathbf{R}, \boldsymbol{\Theta}, \sigma, \tilde{\mathbf{E}}, \tilde{\mathbf{I}} \mid \mathbf{x}^*, \mathbf{t}^*, \mathbf{s}^*) \propto P(\mathbf{x}^*, \mathbf{t}^*, \mathbf{s}^* \mid \mathbf{R}, \boldsymbol{\Theta}, \tilde{\mathbf{E}}, \tilde{\mathbf{I}}) P(\tilde{\mathbf{E}}, \tilde{\mathbf{I}} \mid \boldsymbol{\Theta}, \mathbf{R}) P(\mathbf{R} \mid \sigma) P(\boldsymbol{\Theta}, \sigma)$$

via Markov chain Monte Carlo, then we sample from

$$P(\mathbf{s}^* \mid \mathbf{R}, \boldsymbol{\Theta}, \sigma, \tilde{\mathbf{E}}, \tilde{\mathbf{I}}, \mathbf{x}^*, \mathbf{t}^*)$$

via Monte Carlo by sequentially sampling the latent states directly as described in the following section.

To sample the effective reproduction number and other population parameters via MCMC, we use elliptical slice sampling [Murray et al., 2010] with the augmented likelihood derived in the previous section, with a few modifications. After proposing a vector of parameters values, we obtain the values of $\tilde{E}(t)$ and $\tilde{I}(t)$ by solving the ordinary differential equation version of the EI population process described in Appendix Section A.2 and the next section. In our case, $P(\tilde{\mathbf{E}}, \tilde{\mathbf{I}} \mid \boldsymbol{\Theta}, \mathbf{R})$ is always equal to 1. The vector of parameter values and population size trajectories are then accepted jointly in the elliptical slice sampling algorithm. Further, we assign 0 likelihood to parameters which result in population counts exceeding 8 billion. We also assign 0 likelihood to parameters which result in there being fewer members of the population than there are sampled lineages at the pre-specified times which contribute to the likelihood. The modified ESS algorithm is described in Algorithm 1 in the Appendix.

2.5.2 ODE Approximation of the MJP

The system of equations which describes the deterministic approximation is

$$\begin{aligned} \frac{dE}{du} &= \alpha I - \gamma E, \\ \frac{dI}{du} &= \gamma E - \nu I. \end{aligned}$$

In general, the system of ODEs can be thought of as the large population limit of the Markov Jump Process version of the EI population process [Kurtz, 1971, Britton and Pardoux, 2019]. We solve this system of equations using the closed form solution derived in Goldstein et al. [2025], which in this case happens to be the solution to the conditional means of the Markov Jump Process. For our model, we assume initial conditions and allow α to be a piecewise constant time-varying parameter $\alpha(u)$ and then solve the ODE at the grid times \mathbf{t}^* . We assume E and I are piecewise constant between grid times.

2.5.3 Sampling latent states

Define S_i to be the random variable denoting the state of the process at the i th grid point at time t_i . The target conditional posterior distribution is

$$P(S_i = s_i \mid S_{i-1} = s_{i-1}, T_{i-1} = t_{i-1}, T_i = t_i, X_i = x_i, \alpha, \gamma, \mathbf{E}, \mathbf{I}).$$

Following the phase type framework described above, the joint density of T_i, S_i given $T_{i-1}, S_{i-1}, X_i, \alpha, \gamma, \mathbf{E}, \mathbf{I}$ is simply $f_{s_{i-1}, s_i}(t_i - t_{i-1}, x_i)$. By definition of conditional probability, then, we can calculate the conditional posterior as

$$P(S_i = s_i \mid S_{i-1}, T_{i-1}, T_i, X_i, \alpha, \gamma, \mathbf{E}, \mathbf{I}) = \frac{f_{s_{i-1}, s_i}(t_i - t_{i-1}, x_i)}{\sum_j f_{s_{i-1}, s_j}(t_i - t_{i-1}, x_i)}.$$

Because we assume that individuals are only sampled in state I, S_0 is always known. This allows us to sample from the conditional posterior sequentially.

2.6 Simulation Protocol

We simulate epidemics using a forward-time agent based stochastic SEIR model. An agent based SEIR model is an N -dimensional continuous time Markov chain, where N is the fixed population size. Each individual in the population can be in any of four states, S susceptible to infection, E infected but not yet infectious, I infectious, or R recovered/removed (no longer infectious). We use $\mathbf{G}(u)$ to denote the vector that records the states of all N individuals in the population. If $\mathbf{G}(u)_i$ is S , then the i th individual is susceptible at time u . The process transitions from state \mathbf{G} to state \mathbf{G}' with rates:

$$\lambda_{\mathbf{G}\mathbf{G}'} = \begin{cases} \beta_u/N \times I(u) & \text{if } \mathbf{G}_j = S \text{ and } \mathbf{G}'_j = E \\ \gamma & \text{if } \mathbf{G}_j = E \text{ and } \mathbf{G}'_j = I \\ \nu & \text{if } \mathbf{G}_j = I \text{ and } \mathbf{G}'_j = R \\ 0 & \text{otherwise} \end{cases}$$

Here, $I(u)$ is the total number of individuals in state I at time u . We use the Gillespie algorithm [Gillespie, 1977] to simulate realizations of this model. When aggregated to a population level, this model is equivalent to the commonly used population-level SEIR model.

We modify the algorithm to track infection histories, each time an individual becomes infected (changes from S to E), we choose an individual in state I uniformly at random to be their infection source and record the infection history of the newly infected individual. For each individual, we also record the times they became infected, infectious, and recovered.

For the population SEIR model, the basic reproduction number, R_0 , and effective reproduction number, R_u , are defined as

$$R_{0,u} = \frac{\beta_u}{\nu}, R_u = R_{0,u} \times \frac{S(u)}{N},$$

where $S(u)$ is the total number of individuals susceptible at time u . The basic reproduction number, $R_{0,u}$ is the average number of individuals an individual infected at time u would subsequently infect in a completely susceptible population. The effective reproduction number R_u is the average number of individuals an individual infected at time u would subsequently infect if conditions remained the same as they were at time u . By setting $\alpha(u) = \beta_u S(u)/N$, we are still able to calculate R_u using the EI model. The parameter $1/\gamma$ is the average time spent infected but not infectious, it was set to 4 for all simulations. Likewise the parameter $1/\nu$ is the average time spent infectious, it was set to 7 for all simulations. The total population size was $N = 15000$, with one individual starting in state I and all other individuals starting in state S .

Simulations were run for 22 weeks, and the last date of sampling was one day before 22 weeks. We simulated three separate R_u trajectories, in the first setting (Fixed), $R_{0,u}$ was set at 2.2. This trajectory represents a situation where a new disease is introduced into a susceptible population and no behavior changes or health interventions occur. In the second trajectory (Increase), $R_{0,u}$ changed from 1.3 to 2.3 over a five week period. This trajectory represents a situation where a disease becomes suddenly much more infectious, due to lifting of public health interventions, or changes in population behavior. In the final trajectory (Control), $R_{0,u}$ was set to 2.2 and then changed to 1.1 12 weeks into the simulation, representing a sudden public health intervention which rapidly reduces infectiousness.

For each trajectory, we use two sampling schemes. In isochronous sampling (Iso), all samples are taken at the last date of sampling. In heterochronous (Het) sampling, some number of samples are sampled uniformly at random in the five week interval prior to the last date of sampling. Once an individual has been sampled, any subsequent individuals infected by the sampled individual (directly or indirectly) after the date of sampling cannot be sampled during subsequent sampling. For each type of sampling, we sampled either 50 or 100 total individuals from the currently infectious population completely at random. Starting from the last sampling time, a coalescent tree is formed deterministically using the infection histories of sampled individuals. The data given to the model are the coalescent and sampling times, as well as the number of lineages sampled at each time. For each trajectory, sampling scheme, and number of samples (twelve total scenarios), we simulated fifty trees. An example epidemic realization, R_u curve, and genealogy are shown in Appendix Figure B4. Posterior distribution summaries were estimated using MCMC runs initially of length 100000 or 150000 with the first half discarded as burn in, thinned by every 10th/15th sample. Models were run until parameters had an ESS, tail ESS and bulk ESS of at least 100 [Vehtari et al., 2021]. As needed, the model was rerun with increased

iterations and/or using a different seed. All code needed to reproduce the analyses in this paper are available at https://github.com/igoldsteinh/ei_coal.

3 Results

3.1 Fidelity of the EI Coalescent Approximation

To evaluate the fidelity of our derived EI coalescent model, we empirically compared the distributions of the true EI coalescent times and their distribution under our model. We simulated 1000 population trajectories from the individual (forward) EI population process (equivalent to the process described in section 2.6 for EI rather than SEIR models). Population processes were simulated with $\alpha = 2/3$, $\nu = 1/3$, $\gamma = 1/2$, with one individual initially in the I compartment. Simulations were run till time 35, at which point they were rejected if there were less than 5 infectious individuals in the population. If accepted, 5 infectious individuals were sampled uniformly at random, and their genealogy constructed deterministically using the known history of each individual (Empirical). Then, using the same population trajectories, an EI coalescent tree was simulated using the rate parameters of the model derived in Theorem 2.3 via time transformation [Slatkin and Hudson, 1991, Hein et al., 2004] (TT). However, we rejected any simulations where the number of sampled lineages exceeded the corresponding population count, matching the model actually used for inference. Finally, a coalescent tree was simulated using the solution to the ODE rather than the true population trajectories (TT ODE).

The results of our simulation experiments are shown in Figure 2. The distributions of the intercoalescence intervals under the true EI genealogies generally match that of the derived EI coalescent model when using the true population trajectories. However, when we instead use the ODE solution to simulate coalescent times, the distribution of coalescent times is more biased for some intervals. This is likely a result of the ODE solution not capturing the variation in the stochastic realizations of the EI population process. Appendix Figure B1 shows the ODE solution and ten of the 1000 stochastic realizations previously described. At time 35, the ODE solution has approximately 250 individuals in both the E and I compartments, while the stochastic realizations range from over 1000 to less than 100 individuals in the E and I compartments.

3.2 Simulation Results

We simulated epidemics and coalescent genealogies using a forward-time agent based stochastic SEIR models which track individual infection histories. Using the simulated histories we then reconstructed true coalescent trees. We simulated under three different R_u curves (Fixed, Increase and Control), two sampling schemes (Isochronous and Heterechronous) and two sample sizes (fifty and one hundred). There were fifty simulations for each of the twelve settings, full details are available in the methods section. Examples of the six simulations with fifty sampled lineages are visualized in Appendix Figure B3. The model's credible intervals successfully cover the true trajectories, although depending on the sampled tree, there can be wide uncertainty near the present day. We conjecture this uncertainty is a function of the number of coalescent events close to the present day. An example where the model can become both biased and more uncertain in the absence of coalescent events near the present day is shown in Appendix Figure B6. Examples of the six simulations with one hundred sampled lineages are visualized in Appendix Figure B5.

We summarize model performance across fifty simulations for each scenario using frequentist metrics summarized in Table 1. Envelope (ENV) is a measure of coverage, and is the proportion of time points for which an 95% credible interval from the posterior distribution captured the true value of interest. Mean credible interval width (MCIW) is the mean of 95% credible interval widths across time points within a simulation. Absolute deviation (AD) is a measure of bias, and is the mean of the absolute difference between the posterior median and the true value at each time point. We measure these quantities for each simulation using a grid of true R_u values with a half-daily time-scale. Overall, we see that, as expected, with more sampled lineages, the model has lower deviation, narrower credible intervals, and reasonable, though often conservative coverage. With fifty lineages, the model still has generally good coverage, although performance can vary substantially for any particular simulation.

Empirical vs Time Transformation

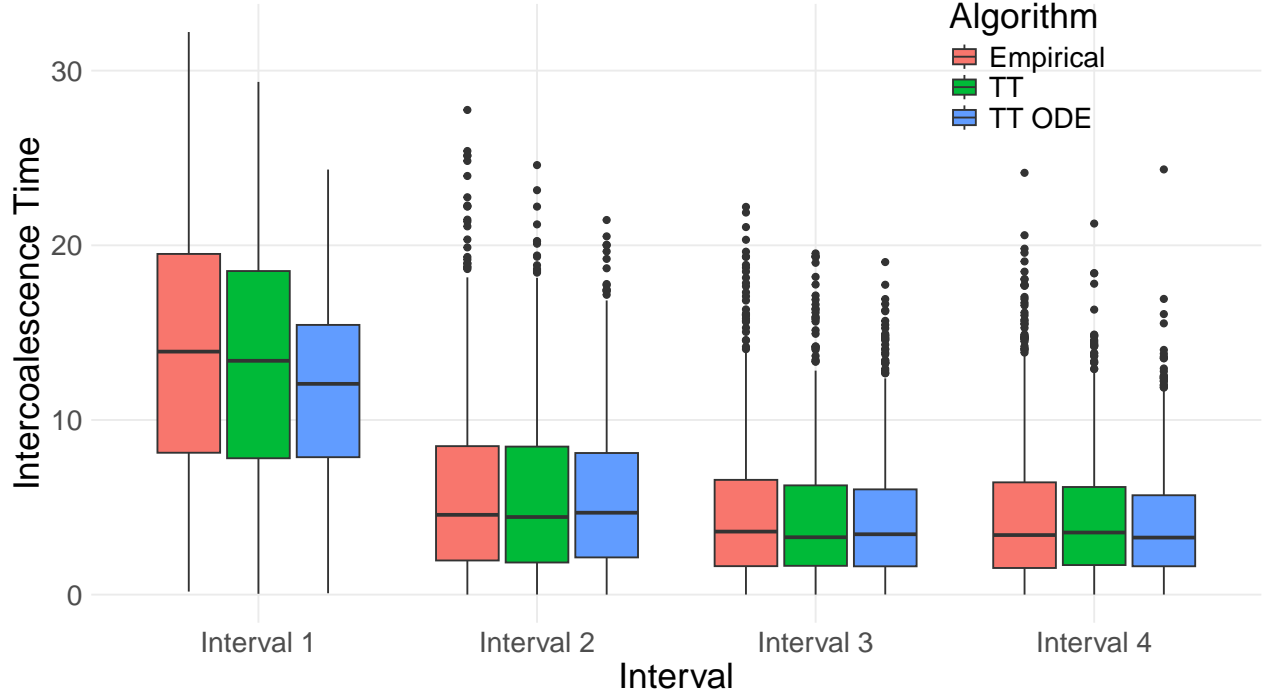


Figure 2: Distribution of intercoalescent intervals for 1000 true EI genealogies and 1000 approximate EI coalescent genealogies. Red (Empirical) boxes show the distribution for the true EI genealogies. Green (TT) boxes show the distribution for the observed EI coalescent genealogies generated via time transformation. Blue (TT ODE) boxes show the distribution for the partially observed coalescent genealogies using the ODE solution rather than the true stochastic trajectory. Genealogies are for five sampled individuals, thus there are 4 total coalescent times, and 4 intercoalescent intervals. Intervals are ordered in backwards time, so that the end of interval 4 is the time to the most recent common ancestor of the genealogy.

3.3 The Effective Reproduction number of Ebola in Liberia

Ebola disease is a severe illness caused by Ebola virus, which can spread from infected animals to humans, as well as from human to human transmission, resulting in regular outbreaks [World Health Organization, 2025]. It is well known to have a significant latent period, plausibly between 6 and 11 days on average [Chowell and Nishiura, 2014, Velásquez et al., 2015]. During the 2013 - 2016 Ebola epidemic in West Africa, more than 28000 cases and 11000 deaths were reported in the countries of Guinea, Liberia and Sierra Leone [World Health Organization, 2016]. In Tang et al. [2023], the authors inferred the time-varying basic reproduction number (Section 2.6) from a pruned posterior tree of Ebola pathogen genomes constructed in Dudas et al. [2017] using a coalescent model for the SIR epidemic model, which has no latent period and assumes individuals become infectious as soon as they are infected. We conduct a similar analysis by estimating a maximum clade credibility tree of the two hundred and eight Liberia sequences collected from the time period used in Tang et al. [2023] (June 20th 2014 through February 14th 2015) collected in Dudas et al. [2017] and using that tree as input for our model. We estimate the maximum clade credibility tree using BEAST X [Baele et al., 2025] using the exact model specified in Dudas et al. [2017]. In brief: the model used an HKY substitution model with four independent regions (codon positions one, two, three and non-coding intergenic regions), a relaxed molecular clock, and a non-parametric coalescent ‘Skygrid’ model with one hundred change points [Gill et al., 2013]. Full details are available in Dudas et al. [2017]. We assume this maximum clade credibility tree (MCC tree) is our data, and infer the effective reproduction number using our EI Coalescent model.

For the EI Coalescent model, we used similar priors to those chosen in Tang et al. [2023]. The prior for R_u was centered at 0.7, and the random walk standard deviation which was centered at 0.05. We chose to let R_u

Sim	ENV	AD	MCIW
Fix. Iso N=50	0.98 (0.66, 1.00)	0.22 (0.17, 0.48)	1.19 (1.02, 1.92)
Fix. Iso N=100	0.96 (0.93, 0.98)	0.18 (0.15, 0.26)	0.96 (0.90, 1.07)
Fix. Het N=50	0.93 (0.59, 1.00)	0.27 (0.18, 0.80)	1.34 (1.10, 2.80)
Fix. Het N=100	0.96 (0.77, 0.98)	0.20 (0.16, 0.27)	1.02 (0.96, 1.17)
Inc. Iso N=50	0.99 (0.73, 1.00)	0.24 (0.14, 0.52)	1.38 (1.10, 2.20)
Inc. Iso N=100	0.99 (0.76, 1.00)	0.17 (0.12, 0.30)	1.09 (0.96, 1.34)
Inc. Het N=50	0.98 (0.75, 1.00)	0.27 (0.16, 0.67)	1.48 (1.16, 2.59)
Inc. Het N=100	0.99 (0.75, 1.00)	0.19 (0.13, 0.37)	1.16 (0.97, 1.44)
Ctrl Iso N=50	0.99 (0.92, 1.99)	0.17 (0.12, 0.26)	1.19 (0.97, 1.44)
Ctrl Iso N=100	0.98 (0.94, 1.00)	0.16 (0.13, 0.22)	0.94 (0.89, 1.03)
Ctrl Het N=50	1.00 (0.85, 1.00)	0.17 (0.11, 0.39)	1.27 (1.06, 1.83)
Ctrl Het N=100	0.98 (0.90, 1.00)	0.16 (0.13, 0.23)	0.96 (0.87, 1.05)

Table 1: Summaries of frequentist metrics of model performance across fifty simulations. For the last three columns the first number is the medians, the numbers in parentheses are the 2.5% and 97.5% quantiles. Envelope (ENV) is a measure of coverage, and ideally should be 0.95. Absolute deviation (AD) is a measure of bias, smaller is better. Mean credible interval width (MCIW) summarises the widths of the 95% credible intervals.

change on a weekly basis, the Tang et al. [2023] analysis divided their time period into 40 equal intervals of length 6.9 days. The prior for the infectious period was centered at seven days, and based on a prior analysis of Ebola in West Africa, we chose to also center the prior of the latent period at seven days [Fintzi et al., 2022]. The full details of prior specification used for the analysis are available in Appendix Table 2. Our maximum clade credibility tree (MCC tree) and posterior inference of the effective reproduction number are shown in Figure 3. In the previous analysis, Tang et al. [2023] found the initial basic reproduction number was plausibly between 1.29 and 2.24, our upper bound for the initial effective reproduction number is substantially smaller, although overall we still find that the initial effective reproduction number is very likely to be above one. In addition to inferring different quantities, the two analyses are not directly comparable, as our MCC tree is not the same as the one used in Tang et al. [2023] (which was not available to directly analyze), and their analysis begins around May of 2014, while ours begins in February of 2014. Despite this difference, the broad trends of the two analyses are similar, as both our analyses agree R_u was likely below one by October 2014.

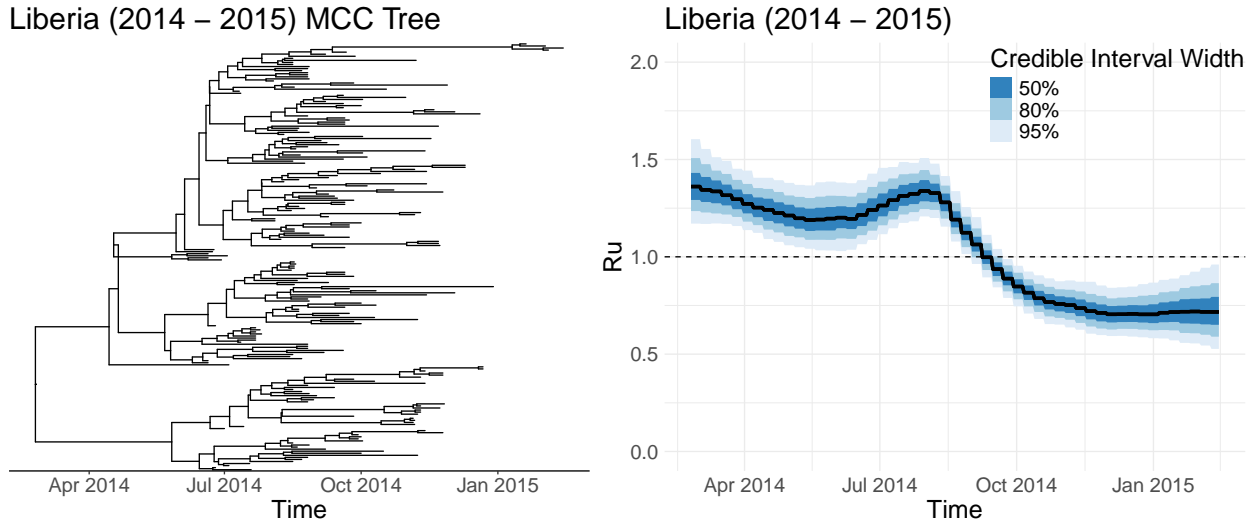


Figure 3: Maximum clade credibility tree and posterior summaries of the effective reproduction number for the 2014 Ebola epidemic in Liberia. In the right plot, black lines are posterior medians, blue shaded areas represent varying levels of credible intervals.

4 Discussion

In this paper we constructed the joint EI population and coalescent process, and an approximate model, the EI coalescent model, suitable for inference. We tested the performance of the inference model on simulations using fixed trees, demonstrating the model’s general good performance. We applied our method to reanalyze the 2014 Ebola outbreak in Liberia, obtaining parameter estimates within a plausible range of known behavior of Ebola and in agreement with previous analyses. Ebola is a good disease for our model, as it is well known to have a significant latent period [Velásquez et al., 2015].

While previous work derived coalescent models for compartmental deterministic systems [Volz, 2012], and more recent work connects coalescent models to stochastic single-type birth-death processes [Crespo et al., 2021], our work contributes in extending these previous efforts by considering a stochastic two-type birth-death process, the EI population process. Our construction of the joint process as a marked point process helps to clarify the nature of coalescent models for epidemic population processes and in particular, clarifies key differences to other approaches such as BDS processes. The techniques used to construct the joint EI population and coalescent process can be easily extended to other common epidemic models, such as the SEIR model.

Although our experiments show that our proposed method has good empirical performance, we observed some discrepancy between the true coalescent distribution and the coalescent distribution using the ODE solution (Figure 2). A stochastic model for the latent trajectories, such as a linear noise approximation [Tang et al., 2023] might further improve model performance, albeit at the cost of increased computational burden.

In general we observed good robustness performance, that is our model performed well in terms of frequentist metrics when fit to genealogies generated using a different data generating model. This is a positive sign the model will perform well under non-trivial model misspecification. However, model performance can vary depending on the shape of the R_u curve and the sampling scheme (Table 1). We hypothesize one driver of variable performance is how the coalescent events are distributed across time. If there are few coalescent events, the model may be unable to differentiate between a scenario where $E(t)$ and $I(t)$ are large, and a scenario when $\alpha(t)$ is small.

The likelihood as written is evaluated via repeated matrix exponentiation, which is computationally expensive [Moler and Van Loan, 2003]. At this time, we do not recommend using this model for trees with more than a few hundred tips. A future direction is to explore augmenting the entire EI coalescent process via uniformization so that the augmented likelihood does not involve matrix exponentiation.

Many of the parameters of the model, as with other compartmental models, are not identifiable, and we rely on informative priors to produce useful inference (Appendix B7). This is typical for this inference problem, for most models which infer the effective reproduction number, the generation time distribution, a function of the latent and infectious periods [Svensson, 2007], is fixed based on prior analyses, see for instance the popular EpiNow2 package [Abbott et al., 2020]. Data integration may help make more model parameters identifiable, since our model conditions on the latent states of the epidemic process, it could be easily adapted to conduct joint inference from a genealogy and other typical data sources such as counts of cases or hospitalizations.

Finally, our method assumes a given genealogy is available without error. This is an unrealistic situation since genealogies are usually not directly observed. In future research, we plan to incorporate our methodology within BEAST to estimate model parameters and population trajectories from molecular sequences directly.

5 Acknowledgments

I.H.G was supported by a Stanford Center for Computational, Evolutionary and Human Genomics Fellowship. J.A.P. acknowledges support from the NSF Career Award #2143242 and NIH Award R35GM148338. Thanks to Nicola Muller for helpful discussion.

References

S. Abbott, J. Hellewell, R. N. Thompson, K. Sherratt, H. P. Gibbs, N. I. Bosse, J. D. Munday, S. Meakin, E. L. Doughty, J. Y. Chun, et al. Estimating the time-varying reproduction number of SARS-CoV-2 using national and subnational case counts [version 2; peer review: 1 approved with reservations]. *Wellcome Open Res* 2020, 5:112, 5(112):112, 2020. URL <https://doi.org/10.12688/wellcomeopenres.16006.2>.

S. W. Attwood, S. C. Hill, D. M. Aanensen, T. R. Connor, and O. G. Pybus. Phylogenetic and phylodynamic approaches to understanding and combating the early SARS-CoV-2 pandemic. *Nature Reviews Genetics*, 23(9):547–562, 2022.

G. Baele, X. Ji, G. W. Hassler, J. T. McCrone, Y. Shao, Z. Zhang, A. J. Holbrook, P. Lemey, A. J. Drummond, A. Rambaut, et al. BEAST X for Bayesian phylogenetic, phylogeographic and phylodynamic inference. *Nature Methods*, pages 1–4, 2025.

T. Britton and E. Pardoux. Stochastic epidemics in a homogenous community. In T. Britton and E. Pardoux, editors, *Stochastic Epidemic Models with Inference*, Lecture Notes in Mathematics (LNM), volume 2255, pages 3–119. Springer, 2019.

L. Cappello, J. Kim, S. Liu, and J. A. Palacios. Statistical challenges in tracking the evolution of SARS-CoV-2. *Statistical science: a review journal of the Institute of Mathematical Statistics*, 37(2):162, 2022.

G. Chowell and H. Nishiura. Transmission dynamics and control of ebola virus disease (evd): a review. *BMC medicine*, 12(1):196, 2014.

F. F. Crespo, D. Posada, and C. Wiuf. Coalescent models derived from birth–death processes. *Theoretical Population Biology*, 142:1–11, 2021.

D. J. Daley and D. Vere-Jones. *An introduction to the theory of point processes: volume I: elementary theory and methods*. Springer, 2003.

G. Didier and S. Guindon. *Models and methods for biological evolution: mathematical models and algorithms to study evolution*. John Wiley & Sons, 2024.

G. Dudas, L. M. Carvalho, T. Bedford, A. J. Tatem, G. Baele, N. R. Faria, D. J. Park, J. T. Ladner, A. Arias, D. Asogun, et al. Virus genomes reveal factors that spread and sustained the Ebola epidemic. *Nature*, 544 (7650):309–315, 2017.

J. Fintzi, J. Wakefield, and V. N. Minin. A linear noise approximation for stochastic epidemic models fit to partially observed incidence counts. *Biometrics*, 78(4):1530–1541, 2022.

M. S. Gill, P. Lemey, N. R. Faria, A. Rambaut, B. Shapiro, and M. A. Suchard. Improving Bayesian population dynamics inference: a coalescent-based model for multiple loci. *Molecular biology and evolution*, 30(3):713–724, 2013.

D. T. Gillespie. Exact stochastic simulation of coupled chemical reactions. *The Journal of Physical Chemistry*, 81(25):2340–2361, 1977.

I. H. Goldstein, D. M. Parker, S. Jiang, and V. M. Minin. Semiparametric inference of effective reproduction number dynamics from wastewater pathogen surveillance data. *Biometrics*, 80(3):ujae074, 2024.

I. H. Goldstein, D. M. Parker, S. Jiang, A. R. Pappu, and V. M. Minin. The signal is not flushed away: Inferring the effective reproduction number from wastewater data in small populations. *arXiv preprint arXiv:2508.03959*, 2025.

J. Hein, M. Schierup, and C. Wiuf. *Gene genealogies, variation and evolution: a primer in coalescent theory*. Oxford University Press, USA, 2004.

N. J. Higham. The scaling and squaring method for the matrix exponential revisited. *SIAM Journal on Matrix Analysis and Applications*, 26(4):1179–1193, 2005.

A. Hobolth, I. Rivas-González, M. Bladt, and A. Futschik. Phase-type distributions in mathematical population genetics: An emerging framework. *Theoretical Population Biology*, 2024.

A. A. King, Q. Lin, and E. L. Ionides. Exact phylodynamic likelihood via structured Markov genealogy processes. *ArXiv*, pages arXiv–2405, 2025.

J. F. C. Kingman. The coalescent. *Stochastic processes and their applications*, 13(3):235–248, 1982.

J. F. C. Kingman. *Poisson processes*, volume 3. Clarendon Press, 1992.

D. Kühnert, T. Stadler, T. G. Vaughan, and A. J. Drummond. Phylodynamics with migration: a computational framework to quantify population structure from genomic data. *Molecular biology and evolution*, 33(8):2102–2116, 2016.

T. G. Kurtz. Limit theorems for sequences of jump Markov processes approximating ordinary differential processes. *Journal of Applied Probability*, 8(2):344–356, 1971.

B. H. Lindqvist. Phase-type models for competing risks, with emphasis on identifiability issues. *Lifetime Data Analysis*, 29(2):318–341, 2023.

M. Möhle. Ancestral processes in population genetics—the coalescent. *Journal of Theoretical Biology*, 204(4):629–638, 2000.

C. Moler and C. Van Loan. Nineteen dubious ways to compute the exponential of a matrix, twenty-five years later. *SIAM Review*, 45(1):3–49, 2003.

N. F. Müller, D. A. Rasmussen, and T. Stadler. The structured coalescent and its approximations. *Molecular biology and evolution*, 34(11):2970–2981, 2017.

I. Murray, R. Adams, and D. MacKay. Elliptical slice sampling. In *Proceedings of the thirteenth international conference on artificial intelligence and statistics*, pages 541–548. JMLR Workshop and Conference Proceedings, 2010.

J. Niesen and W. Wright. A Krylov subspace algorithm for evaluating the φ -functions in exponential integrators. *arXiv preprint arXiv:0907.4631*, 2009.

C. Rackauckas and Q. Nie. Differentialequations.jl – a performant and feature-rich ecosystem for solving differential equations in julia. *The Journal of Open Research Software*, 5(1), 2017. doi: 10.5334/jors.151. URL <https://app.dimensions.ai/details/publication/pub.1085583166> and <http://openresearchsoftware.metajnl.com/articles/10.5334/jors.151/galley/245/download/>. Exported from <https://app.dimensions.ai> on 2019/05/05.

D. A. Rasmussen, O. Ratmann, and K. Koelle. Inference for nonlinear epidemiological models using genealogies and time series. *PLOS Computational Biology*, 7(8):e1002136, 2011.

M. Salemi, A.-M. Vandamme, and P. Lemey. *The phylogenetic handbook: a practical approach to phylogenetic analysis and hypothesis testing*. Cambridge University Press, 2009.

M. Slatkin and R. R. Hudson. Pairwise comparisons of mitochondrial DNA sequences in stable and exponentially growing populations. *Genetics*, 129(2):555–562, 1991.

T. Stadler. Sampling-through-time in birth–death trees. *Journal of theoretical biology*, 267(3):396–404, 2010.

A. Svensson. A note on generation times in epidemic models. *Mathematical Biosciences*, 208(1):300–311, 2007.

M. Tang, G. Dudas, T. Bedford, and V. N. Minin. Fitting stochastic epidemic models to gene genealogies using linear noise approximation. *The annals of applied statistics*, 17(1):1, 2023.

S. Tavaré and O. Zeitouni. *Lectures on probability theory and statistics: Ecole d'Eté de Probabilités de Saint-Flour XXXI-2001*. Springer, 2004.

T. G. Vaughan and T. Stadler. Bayesian phylodynamic inference of multitype population trajectories using genomic data. *Molecular Biology and Evolution*, 42(6):msaf130, 2025.

A. Vehtari, A. Gelman, D. Simpson, B. Carpenter, and P.-C. Bürkner. Rank-normalization, folding, and localization: An improved R for assessing convergence of MCMC (with discussion). *Bayesian analysis*, 16(2):667–718, 2021.

G. E. Velásquez, O. Aibana, E. J. Ling, I. Diakite, E. Q. Mooring, and M. B. Murray. Time from infection to disease and infectiousness for Ebola virus disease, a systematic review. *Clinical Infectious Diseases*, 61(7):1135–1140, 2015.

E. M. Volz. Complex population dynamics and the coalescent under neutrality. *Genetics*, 190(1):187–201, 2012.

E. M. Volz and I. Siveroni. Bayesian phylodynamic inference with complex models. *PLoS computational biology*, 14(11):e1006546, 2018.

E. M. Volz, S. L. Kosakovsky Pond, M. J. Ward, A. J. Leigh Brown, and S. D. Frost. Phylodynamics of infectious disease epidemics. *Genetics*, 183(4):1421–1430, 2009.

World Health Organization. Ebola situation report—10 june 2016. <https://iris.who.int/server/api/core/bitstreams/215feb7c-6e72-42fe-85e3-4c3dc6249472/content>, 2016. Accessed: 2025-11-05.

World Health Organization. Ebola virus disease. <https://www.who.int/news-room/fact-sheets/detail/ebola-disease>, 2025. Accessed: 2025-11-05.

H. Xin, Y. Li, P. Wu, Z. Li, E. H. Lau, Y. Qin, L. Wang, B. J. Cowling, T. K. Tsang, and Z. Li. Estimating the latent period of coronavirus disease 2019 (COVID-19). *Clinical Infectious Diseases*, 74(9):1678–1681, 2022.

K. Zeng, B. Charlesworth, and A. Hobolth. Studying models of balancing selection using phase-type theory. *Genetics*, 218(2):iyab055, 2021.

A Appendix

A.1 Compartmental Models

A.1.1 The SEIR Model

The SEIR model is the traditional model used for a pathogen with a latent period. In this section, we describe it in detail, and show its relationship to the EI model used in the main paper. The SEIR describes an infectious disease outbreak of a homogeneously mixing population, with the population divided into four compartments: susceptible, exposed, infectious, and removed. We represent the SEIR model as a four dimensional continuous time Markov jump process, $\mathbf{G}(\mathbf{u}) = (S(u), E(u), I(u), R(u))$. By construction, $R(u)$ is redundant, as $R(u) = N - S(u) - E(u) - I(u)$, where N is the fixed total population size. The SEIR dynamics are described by rate parameters such that

$$\begin{aligned} P(\mathbf{G}(u + du) = (s - 1, e + 1, i, r) \mid \mathbf{G}(u) = (s, e, i, r)) &= \beta_u is / N du + o(du), \\ P(\mathbf{G}(u + du) = (s, e - 1, i + 1, r) \mid \mathbf{G}(u) = (s, e, i, r)) &= \gamma e du + o(du), \\ P(\mathbf{G}(u + du) = (s, e, i - 1, r + 1) \mid \mathbf{G}(u) = (s, e, i, r)) &= \nu i du + o(du), \\ P(\mathbf{G}(u + du) = (s, e, i, r) \mid \mathbf{G}(u) = (s, e, i, r)) &= 1 - (\beta is / N + \gamma e + \nu i) du + o(du). \end{aligned}$$

Here γ is the inverse of the mean latent period, and ν is the inverse of the mean infectious period. We describe the infectiousness of the disease through the time-varying rate parameter β_u . With this model, the time-varying basic reproduction number, $R_{0,u}$, and effective reproduction number, R_u , are defined as

$$R_{0,u} = \frac{\beta_u}{\nu}, \quad R_u = R_{0,u} \times \frac{S(u)}{N}.$$

The basic reproduction number, $R_{0,u}$ is the expected number of individuals an individual infected at time u would subsequently infect in a completely susceptible population. The effective reproduction number R_u is the expected number of individuals an individual infected at time u would subsequently infect if conditions remained the same as they were at time u . Intuitively, R_u takes into account the fact that some people have already been infected, as it is $R_{0,u}$ multiplied by the fraction of the population which is still susceptible at time u .

A.1.2 The EI Model

The epidemic model used in the main text is the EI model, which is represented as a two dimensional continuous time Markov jump process $\mathbf{H}(u) = (E(u), I(u))$, defined as:

$$\begin{aligned} P(\mathbf{H}(u + du) = (e + 1, i) \mid \mathbf{H}(u) = (e, i)) &= \alpha_u i du + o(du), \\ P(\mathbf{H}(u + du) = (e - 1, i + 1) \mid \mathbf{H}(u) = (e, i)) &= \gamma e du + o(du), \\ P(\mathbf{H}(u + du) = (e, i - 1) \mid \mathbf{H}(u) = (e, i)) &= \nu i du + o(du), \\ P(\mathbf{H}(u + du) = (e, i) \mid \mathbf{H}(u) = (e, i)) &= 1 - (\alpha_u i + \gamma e + \nu i) du + o(du). \end{aligned}$$

In contrast to the SEIR model, there is no S compartment, rather, changes in the susceptibility of the population are incorporated in changes in α_u . Likewise, there is no R compartment, however, the dynamics of recovery remain the same as in the SEIR model, we just don't track the cumulative number of recoveries. The effective reproduction number, R_u is still recoverable by setting $\alpha_u = \beta_u \times \frac{S(u)}{N}$, so that

$$R_u = R_{0,u} \times \frac{S(u)}{N} = \frac{\alpha_u}{\nu}.$$

A.2 Closed Form Solution to the EI ODE System

In [Goldstein et al., 2025], we derived the closed form solution to the EI ODE system for a time interval where α is constant shown below using **Mathematica** (Version 13.1).

$$\begin{aligned} \frac{dE}{du} &= \alpha I - \gamma E, \\ \frac{dI}{du} &= \gamma E - \nu I. \end{aligned}$$

In particular, we treat the solution to the system as the action of the matrix exponential of

$$\mathbf{V}u = \begin{bmatrix} -\gamma u & \alpha u \\ \gamma u & -\nu u \end{bmatrix}$$

on the vector $[E(0), I(0)]$. We then solve this action of the matrix exponential symbolically. We provide the solutions below. Let $B = \sqrt{4\alpha\gamma + (\gamma - \nu)^2}$. Define the following four functions:

$$\begin{aligned} g_1(\gamma, \nu, \alpha, u) &= \frac{4\alpha(1 + e^B)\gamma + (\gamma - \nu)(1 + e^B\gamma + B - \nu - e^B(B + \nu))}{2e^{(\gamma+B+\nu)u/2}(4\alpha\gamma + (\gamma - \nu)^2)}, \\ g_2(\gamma, \nu, \alpha, u) &= \frac{\alpha(-1 + e^B)}{e^{(\gamma+B+\nu)u/2}B}, \\ h_1(\gamma, \nu, \alpha, u) &= \frac{\gamma(-1 + e^B)}{e^{(\gamma+B+\nu)u/2}B}, \\ h_2 &= \frac{4\alpha(1 + e^B\gamma + (\gamma - \nu) * (\gamma - B + e^B B + e^B(\gamma - \nu) - \nu))}{2e^{(\gamma+B+\nu)u/2}(4\alpha\gamma + (\gamma - \nu)^2)}. \end{aligned}$$

Then, given the values of $E(0)$ and $I(0)$, we have

$$\begin{aligned} E(u) &= g_1(\gamma, \nu, \alpha, u)E(0) + g_2(\gamma, \nu, \alpha, u)I(0), \\ I(u) &= h_1(\gamma, \nu, \alpha, u)E(0) + h_2(\gamma, \nu, \alpha, u)I(0). \end{aligned}$$

A.3 Rate Matrix Details for the EI Coalescent Likelihood

Below we include an example \mathbf{A} and \mathbf{L} matrix for $n = 3$ extant lineages for clarity. Again the columns and rows are ordered so that the first column (row) corresponds to the state of all n lineages in state I, decreasing by one from left to right and top to bottom.

$$\begin{aligned} \mathbf{A} &= \begin{bmatrix} -3\frac{\gamma(e+1)}{(i)} & 3\frac{\gamma(e+1)}{(i)} & 0 & 0 \\ (i-2)^+\frac{\alpha}{(e)} & -\left((i-2)^+\frac{\alpha}{e} + 2\frac{\gamma(e+1)}{(i)} + 2\frac{\alpha}{e}\right) & 2\frac{\gamma e}{(i)} & 0 \\ 0 & 2(i-1)^+\frac{\alpha}{(e)} & -\left(2(i-1)^+\frac{\alpha}{(e)} + \frac{\gamma(e+1)}{(i)} + 2\frac{\alpha}{(e)}\right) & 2\frac{\gamma e}{(i)} \\ 0 & 0 & 3i\frac{\alpha}{(e)} & -3i\frac{\alpha}{(e)} \end{bmatrix}. \\ \mathbf{L} &= \begin{bmatrix} 0 & 0 \\ 2\frac{\alpha}{e} & 0 \\ 0 & 2\frac{\alpha}{e} \\ 0 & 0 \end{bmatrix}. \end{aligned}$$

A.4 Alternative EI Augmented Likelihood with Piecewise Time-varying Parameters

In the main paper, we use a model which augments the observed data with the counts of lineages in the E and I compartments at coalescent, sampling, and pre-specified grid times at which $\alpha(t)$ is *a priori* allowed to change. In this way, the likelihood is the product of terms corresponding to number of $\alpha(t)$ changepoints. Alternatively, one can write the augmented likelihood only at coalescent and sampling times, but not at the times when $\alpha(t)$ is assumed to change. In this case, suppose that for the interval that starts at t_{i-1} in state s_{i-1} and ends at time t_i in state s_i that there are J times in the interval during which α changes. We denote the times at which α changes as $t_{i,1}, \dots, t_{i,J-1}$ and $A_{k,j}$ is the matrix of rates for the j th subinterval, likewise $L_{k,j}$ is the corresponding L matrix. Then, by properties of Continuous Time Markov Chains, we can write the likelihood contributions for when $x_i = 1$ as follows:

$$f_{s_{i-1}, s_i}(t_{i-1}, t_{i,1}, \dots, t_{i,J}, t_i, x_i = 1) = \mathbf{e}_{s_{i-1}}^T \exp \mathbf{A}_{k,1}(t_{i,1} - t_{i-1}) \exp \mathbf{A}_{k,2}(t_{i,2} - t_{i,1}) \dots \exp \mathbf{A}_{k,J}(t_i - t_{i,J-1}) \mathbf{l}_{J, s_i}.$$

Likewise, when $x_i = 0$,

$$f_{s_{i-1}, s_i}(t_{i-1}, t_{i,1}, \dots, t_{i,J}, t_i, x_i = 0) = \exp \mathbf{A}_{k,1}(t_{i,1} - t_{i-1}) \exp \mathbf{A}_{k,2}(t_{i,2} - t_{i,1}) \dots \exp \mathbf{A}_{k,J}(t_i - t_{i,J-1})_{s_{i-1}, s_i}.$$

Using this alternate likelihood, less states need to be sampled (augmented), which may improve the efficiency of the MCMC algorithm. To test this empirically, we fit both approaches to the simulated data used in Figure 2 and ran them for 30000 iterations on the same 2022 Macbook M2 Air. The minimum ESS per second for the alternative version of the model was 0.044, versus 0.043 for the main version of the model, suggesting any benefits are not dramatic. Both models are available on the github repo.

A.5 Elliptical Slice Sampling

Let \mathbf{q} be the vector of accepted log scale mean zero parameters, that is \mathbf{q} is the vector of accepted Θ , \mathbf{R} , and σ on the log scale with the prior mean (on the log scale) subtracted from their values. All priors are log-normal, so on the log scale they are normal, and we can write a joint prior normal density with variance matrix Σ . Let μ be those prior means on the log scale. Let $\tilde{\mathbf{E}}, \tilde{\mathbf{I}}$ be the values of $\tilde{E}(t)$ and $\tilde{I}(t)$ needed to evaluate the likelihood for the accepted values \mathbf{q} . Define $L(\mathbf{q}, \tilde{\mathbf{E}}, \tilde{\mathbf{I}}) = \log P(\mathbf{t}, \mathbf{x}, \mathbf{t}^*, \mathbf{s} | \exp \mathbf{q} + \mu, \tilde{\mathbf{E}}, \tilde{\mathbf{I}})$. Further define $V(\tilde{\mathbf{E}}, \tilde{\mathbf{I}}, \mathbf{t}, \mathbf{x}, \mathbf{t}^*, \mathbf{s})$ be a function which is 1 if, for all points t_i in \mathbf{t} and \mathbf{t}^* , $n_E(t_i) \leq \tilde{E}(t_i)$ and $n_I(t_i) \leq \tilde{I}(t_i)$ and 0 otherwise. Finally, let $W(\tilde{\mathbf{E}}, \tilde{\mathbf{I}})$ be a function which is one if $\max \tilde{\mathbf{E}} + \tilde{\mathbf{I}} \leq 8E9$. The modified elliptical slice sampling algorithm [Murray et al., 2010] is as follows:

Algorithm 1 Modified Elliptical Slice Sampling Algorithm with ODE Solution

```

Input Current state  $\mathbf{q}$  prior means  $\mu$ , compartment counts  $\tilde{\mathbf{E}}, \tilde{\mathbf{I}}$ 
Output New state  $\mathbf{q}'$  updated  $\tilde{\mathbf{E}}, \tilde{\mathbf{I}}$ 

1: Sample ellipse:  $\psi \sim N(0, \Sigma)$ 
2: Set log likelihood threshold:
3:  $u \sim \text{Uniform}(0, 1)$ 
4:  $\log y \leftarrow L(\mathbf{q}, \tilde{\mathbf{E}}, \tilde{\mathbf{I}}) + \log u$ 
5: Draw the initial angle
6:  $\theta \sim \text{Uniform}(0, 2\pi)$ 
7:  $[\theta_{min}, \theta_{max}] \leftarrow [\theta - 2\pi, \theta]$ 
8:  $\mathbf{q}' \leftarrow \mathbf{q} \sin \theta + \psi \cos \theta$  ▷ ODE solution according to Section A.2
10: if  $L(\mathbf{q}', \tilde{\mathbf{E}}, \tilde{\mathbf{I}}) > \log y \& V(\tilde{\mathbf{E}}, \tilde{\mathbf{I}}, \mathbf{t}, \mathbf{x}, \mathbf{t}^*, \mathbf{s}) == 1 \& W(\tilde{\mathbf{E}}, \tilde{\mathbf{I}}) == 1$  then
11:   return:  $\mathbf{q}', \tilde{\mathbf{E}}, \tilde{\mathbf{I}}$ 
12: else
13:   Shrink the bracket:
14:   if  $\theta < 0$  then
15:      $\theta_{min} \leftarrow \theta$ 
16:   else
17:      $\theta_{max} \leftarrow \theta$ 
18:   end if
19:    $\theta \sim \text{Uniform}(\theta_{min}, \theta_{max})$ 
20:   Go To 8
21: end if

```

B Results

B.1 Fidelity of the EI Coalescent Approximation

In Figure 2 we showed a comparison of the empirical distribution of coalescent times simulated from the true population dynamics and the empirical distribution of coalescent times simulated according to our proposed EI coalescent model. We argue that the discrepancy is mainly due to the ODE approximation to the population dynamics. In Figure B-1, we show ten stochastic realizations of the EI population process and the ODE solution, providing a range of possible discrepancies between the two models. In contrast, if we change the grid times at which we solve the ODE, the distribution of coalescent intervals remains largely unchanged. We tested this by comparing the distribution of coalescent intervals when simulating using the ODE solution solved at regular grid times (0.5, 1, 1.5, ...) vs the realized change times simulated from the 1000 stochastic realizations of the EI model (Figure B2).

ODE vs Stochastic EI Trajectories

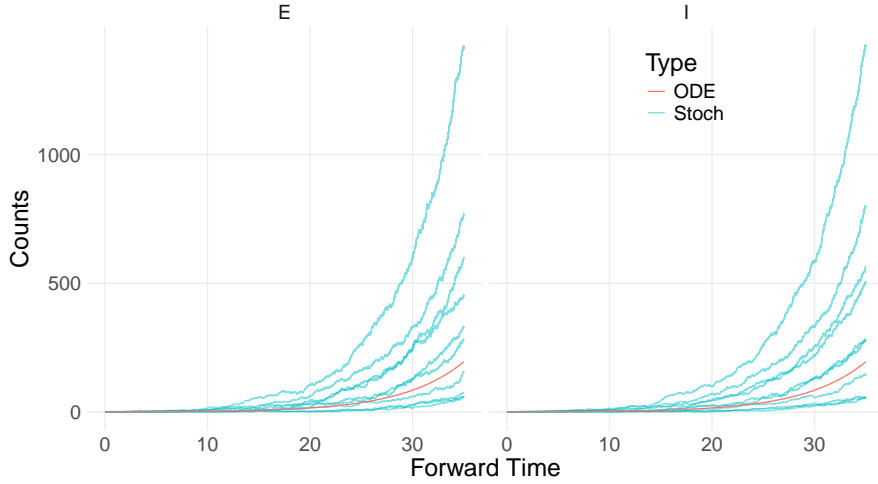


Figure B1: Example with 10 realizations of the stochastic EI population process (blue) and the ODE solution to the deterministic EI process (red).

ODE vs ODE Varying Grid

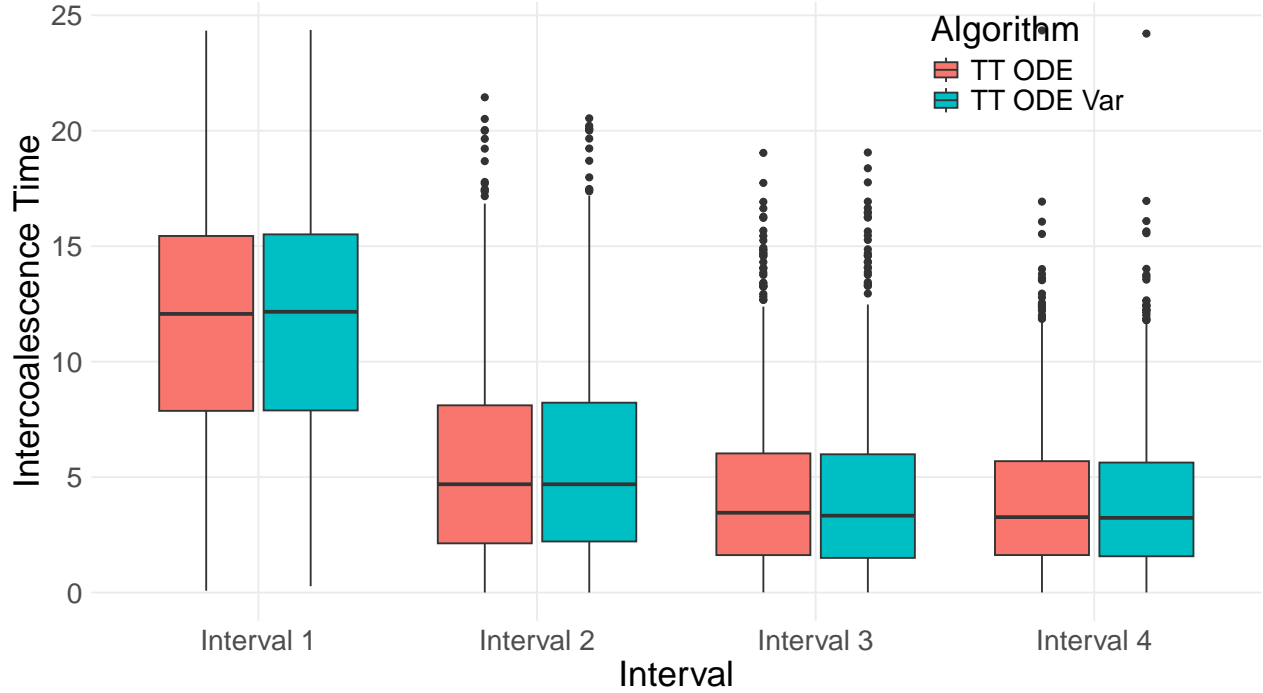


Figure B2: Boxplots of intercoalescent intervals. Red (ODE) boxplots correspond to intercoalescent intervals simulated using an ODE solution solved on a regular grid (0.5, 1, 1.5, ...). Blue (TT ODE Var) boxplots correspond to intercoalescent intervals simulated using the ODE solution solved at the realized times simulated from the 1000 stochastic realizations of the EI process used to construct intervals in Figure 2 of the main text. Phylogenies with five tips are reconstructed, thus there are 4 intercoalescent intervals. Intervals are ordered in backwards time, so that the end of interval 4 is the time to the most recent common ancestor of the phylogeny

B.2 Simulation Results

Examples of the six simulations with fifty sampled lineages are visualized in Figure B3. The model's credible intervals successfully cover the true trajectories, although depending on the sampled tree, there can be wide uncertainty near the present day. Figure B4 shows an example simulated epidemic and sample genealogy. Figure B5 shows examples of the six simulations with 100 sampled lineages.

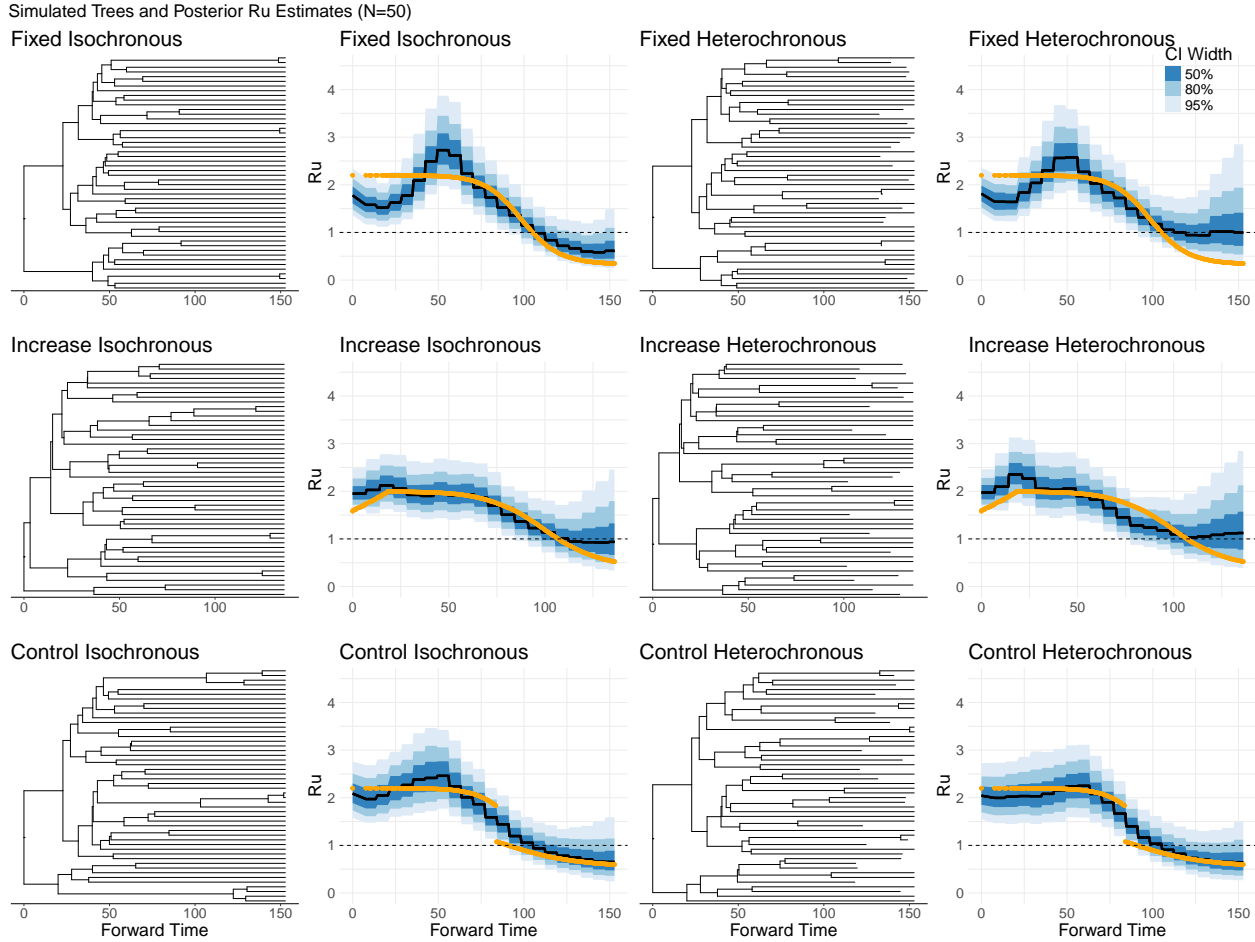


Figure B3: Simulated sampled genealogies and posterior summaries of R_u for simulation scenarios with fifty sampled lineages. First row is the fixed scenario, second is the increase scenario, third row is the control scenario. True R_u values are shown in orange, black lines are posterior medians, blue shaded areas are credible intervals. Time is in forward time, with time 0 being set to the time of the most recent common ancestor. Note the increase scenario has a different time axis, because the time to the most recent common ancestor is consistently smaller than in the other two scenarios.

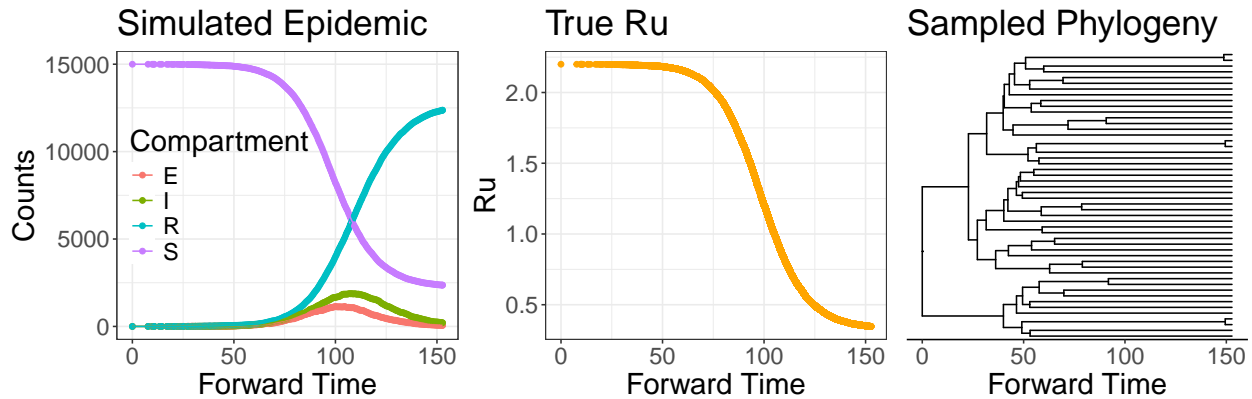


Figure B4: Example of a simulated epidemic, true R_u curve, and sample genealogy. The left-most plot shows the simulated Epidemic, different colors correspond to the counts of individuals in each state on a half-day time grid. The middle panel shows the true R_u curve which is the target of inference. The right panel shows the sample genealogy of 50 lineages. The genealogy was used to infer the posterior estimates of R_u shown in the top row of the second column of Figure B3.

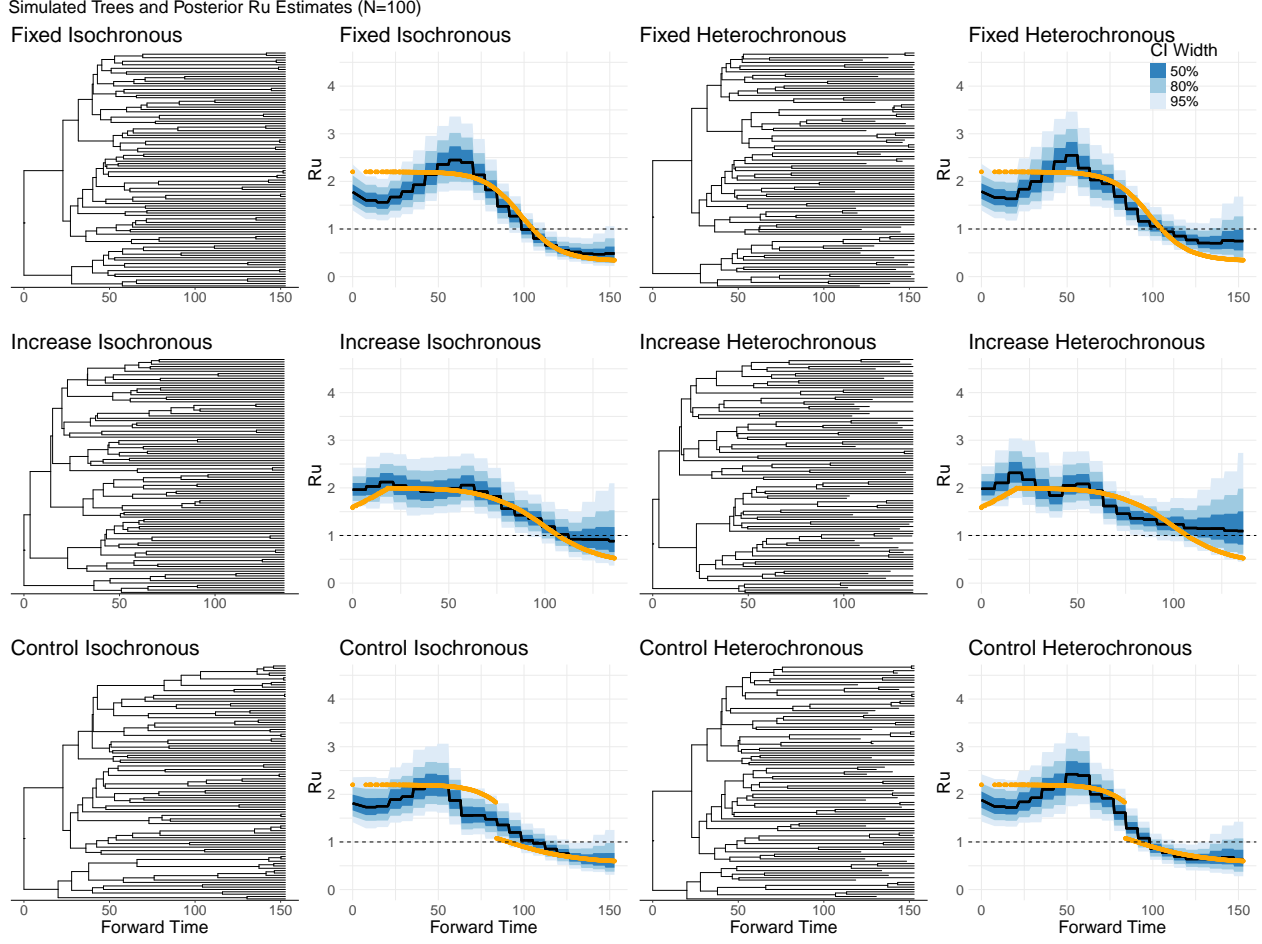
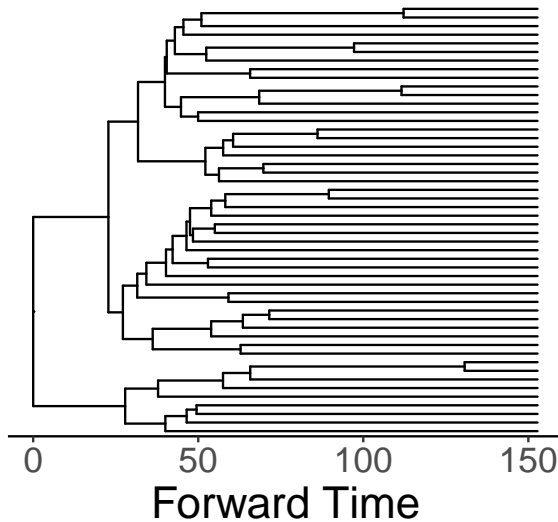


Figure B5: Simulated sampled genealogies and posterior summaries of R_u for simulation scenarios with one hundred sampled lineages. First row is the fixed scenario, second is the increase scenario, third row is the control scenario. True R_u values are shown in orange, black lines are posterior medians, blue shaded areas are credible intervals. Time is in forward time, with time 0 being set to the time of the most recent common ancestor. Note the increase scenario has a different time axis, because the time to the most recent common ancestor is consistently smaller than in the other two scenarios.

B.2.1 Inference Failure

We hypothesize this kind of failure can occur when there are not enough coalescences occurring in a particular region of the genealogy, in the case shown in Appendix Figure B6 there is only one coalescence in the last 30 days of the simulation.

Fixed Isochronous



Fixed Isochronous

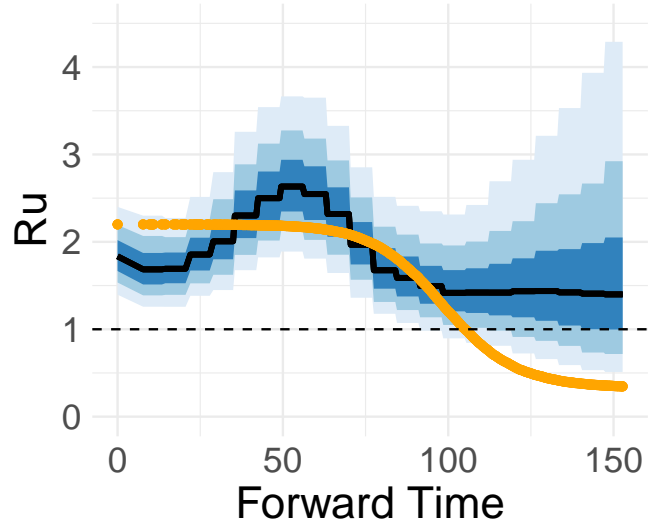


Figure B6: Example of a simulated sampled genealogy from the Fixed Iso simulation where the model fails to cover the true R_u curve. Yellow dots are true R_u values, black lines are posterior medians, blue shaded areas are varying levels of credible intervals (see B3).

B.2.2 Model Priors for Simulations

For the Increase scenario, the prior for R_0 was centered at 1.2 rather than 2, otherwise the priors were the same as the Fixed scenario. The priors for the Control scenario were the same as the Fixed scenario. Because the time to the most recent common ancestor is random, there is no fixed true value of the initial R_u or for the initial counts in the E and I compartments across simulations.

Table B1: Priors used in the Fixed simulation scenarios.

Parameter	Model	Prior	Prior Median (95% Interval)	Truth
γ	All	Log-normal($\log(1/4)$, 0.25)	0.25 (0.15, 0.4)	0.25
ν	All	Log-normal($\log(1/7)$, 0.25)	0.14 (0.09, 0.23)	0.14
σ_{rw}	All	Log-normal($\log(0.2)$, 0.1)	0.2 (0.16, 0.24)	NA
R_0	All	Log-Normal($\log(2.0)$, 0.2)	2.0 (1.35, 2.99)	Varies
$E(0)$	All	Log-Normal($\log(1.1)$, 0.05)	1.1 (0.99, 1.21)	Varies
$I(0)$	All	Log-Normal($\log(1.1)$, 0.05)	1.1 (0.99, 1.21)	Varies

In Figure B7 we compare the prior and posteriors of the fixed parameters of the model. The initial number of latent and infectious individuals, as well as the average latent period and average infectious period are all not identifiable. This is typical for this inference problem unfortunately, for most models which infer the effective reproduction number, the generation time distribution, a function of the latent and infectious periods [Svensson, 2007], is fixed based on prior analyses, see for instance the popular EpiNow2 package [Abbott et al., 2020]. The prior for the random walk standard deviation must likewise be chosen by the user.

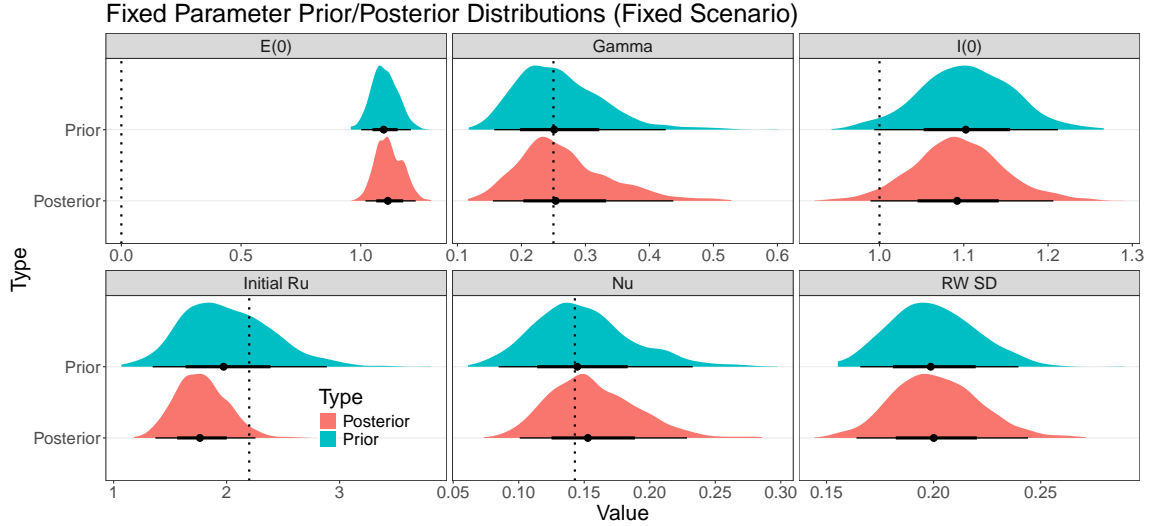


Figure B7: Prior and posterior densities for fixed model parameters. Posterior summaries are from the model fit to the data shown in Figure B3 top left plot of the main text. Blue densities are the prior, red densities are the posterior, dotted lines indicate true values.

B.2.3 Model Priors for Liberia Ebola analysis

For the Ebola analysis, we used priors similar to those used in the analyses of Tang et al. [2023] and Fintzi et al. [2022].

Table B2: Priors for the 2014 Liberia Ebola outbreak.

Parameter	Model	Prior	Prior Median (95% Interval)
γ	All	Log-normal($\log(1/7)$, 0.45)	0.14 (0.06, 0.35)
ν	All	Log-normal($\log(1/7)$, 0.3)	0.14 (0.08, 0.26)
σ_{rw}	All	Log-normal($\log(0.05)$, 0.2)	0.05 (0.03, 0.07)
R_0	All	Log-Normal($\log(0.7)$, 0.5)	0.7 (0.26, 1.87)
$E(0)$	All	Log-Normal($\log(1.1)$, 0.05)	1.1 (0.99, 1.21)
$I(0)$	All	Log-Normal($\log(1.1)$, 0.05)	1.1 (0.99, 1.21)